

Chapter 1

Overview of the Chinese National Key Basic Research Project Entitled “Development and Evaluation of High-Resolution Climate System Models”

Rucong Yu, Tianjun Zhou, Tongwen Wu, Wei Xue
and Guangqing Zhou

Abstract An overview of the Chinese National Key Basic Research Project entitled “Development and Evaluation of High-Resolution Climate System Models” under grant No. 2010CB951900 is presented. The background and the objectives of the project are introduced. The main progress made in the past 5 years of the project is the development of “one system” and “two platforms”, where “one system” refers to the high-resolution modeling system and “two platforms” refers to the multi-model ensemble coupling platform and model evaluation system. The technical details of the high-resolution modeling system and multi-model ensemble coupling platform are summarized. For the model evaluation system, instead of presenting the details of the metrics used in gauging model performances, the observational metrics are used to assess the climate models developed in this project that employ low, middle, and high resolutions. The strengths and weaknesses of adopting a higher model resolution are identified and discussed.

Keywords Climate model · High resolution · Ensemble · Metrics

1.1 Introduction

High-resolution climate system models are important tools for climate change studies, and their development is a key topic within the climate change research community. The sustainable development of economies and society also relies heavily on support from high-resolution modeling, predictions, and projections of the climate, as part of its decision- and policy-making processes.

1.1.1 Demand for the Sustainable Development of Economies and Society

The issue of global climate change, characterized by global warming, has become one of the greatest challenges for the sustainable development of human society. Observations have already shown, through multiple lines of evidence, that the climate is changing across our planet, resulting in the pressing global problem we recognize today. In China, a proper response to the issue of global climate change lies not only in the context of the country's economic and societal sustainable development, but also in that of international political and diplomatic discourse, and the national development strategy.

It is of great importance to develop climate system models to enhance scientific research on climate change. Whether driven by natural or anthropogenic forcing agents, climate change can lead to alterations in the likelihood of occurrence and/or strength of extreme weather and climate events. The coupled climate system model is the most important tool for understanding climate variability and to project future climate change. The capability of a country's climate system model is an objective reflection of its ability to tackle climate change issues. Therefore, climate system model development in China promotes the country's overall ability to contribute to solving the problems of climate change within the global context.

More specifically, the ability to robust model and predict the climate has profound and far-reaching significance for preventing climatic disasters. In economic terms, the cost imposed in China by the major types of climatic disasters, such as drought and flooding, equates to more than 200 billion RMB each year. Moreover, against the background of global warming, the frequency of climatic disasters in China has increased in recent decades. Given the importance of climate system models in predicting climatic anomalies, developing such models and improving their prediction and projection abilities are conducive to preventing and mitigating meteorological disasters.

Previous efforts to develop climate system models in China have laid solid foundations, but a growing gap between the capabilities of such models at the national and international level remains. Therefore, developing high-resolution climate system models is a matter of great urgency in China. Climate system models with high resolutions can distinguish finer spatiotemporal variation of physical processes, and thus make more reliable simulations and predictions. In this sense, the resolution of a model is an important metric to measure its performance. A number of countries in North America and Europe have already launched high-resolution models, but before the establishment in 2010 of the project reported upon in this book, there were no publically released high-resolution climate models in China. The current level of model development and a lack of depth in recognizing and understanding model uncertainties have already affected China's ability to tackle climate change issues. However, the implementation of this project aims to

speed up the development of a high-resolution climate system model in China, and thus combats some of these issues.

Most earth scientists and relevant technical policymakers in China have realized the necessity and urgency of developing climate system models. In recent years, the state has issued a series of plans to promote the development of the climate model. Based on currently existing atmospheric general circulation models (AGCMs), oceanic general circulation models (OGCMs), and the coupled climate models of the National Climate Center (NCC) at the China Meteorological Administration (CMA), and the Institute of Atmospheric Physics (IAP), Chinese Academy of Sciences (CAS), the project encourages collaborations within the Chinese climate modeling community and aims to reduce the gap with the advanced level attained in many other countries of the world active in this field of research.

1.1.2 Scientific Basis for Climate Change Research

The prediction and projection capabilities of current climate system models need to be improved, and developing high-resolution climate models is an important approach to improve their performance. The projection of future climate change based on climate models is the scientific foundation for mitigating and adapting to climate change. Current climate models have a certain capacity in terms of simulating large-scale climate change, but are less capable at simulating regional-scale variation. With the rapid development of high-performance computers, the development of high-resolution climate models has become a central aim for the international climate research community. It is internationally recognized that developing high-resolution models is an important requirement of capacity building to adapt to climate change.

Developing high-resolution climate system models is a key technology for improving the simulation and projection of the East Asian climate. The East Asian monsoon is a distinctive climate phenomenon, but the current mid- and low-resolution climate models demonstrate large biases when simulating the location and seasonal evolution of East Asian monsoon rainfall; in particular, an artificially strong rainfall center on the eastern and southern periphery of the Tibetan Plateau (Yu et al. 2000; Zhou and Li 2002; Chen et al. 2010; Song and Zhou 2014a, b; Yu et al. 2015). Influenced by the complex topography and land-sea distribution, mid- and low-resolution climate models fail to reasonably represent the forcing of the complicated topography, which causes the biases in simulating the atmospheric circulation, and directly affects the simulation of cloud radiative forcings. These biases bring large uncertainties to the model simulations. Therefore, developing a high-resolution climate model is essential for improving the simulation of East Asian climate, especially the simulation of monsoon precipitation, and will provide a foothold for improving short-range climate prediction.

1.1.3 Expected Contributions to Solving Problems at the National Level

Developing high-resolution climate models is at the forefront of international scientific climate system research. It is also a matter of urgency for national diplomatic negotiations and macroeconomic policy-making related to the climate change problem. The present reported project aims to bring together the main climate model research units in China, such as the NCC and IAP, as well as large scientific computation research institutions such as Tsinghua University, thereby drawing upon the accumulation of years of work on climate model development to centralize the strength of the research and make significant contributions to solving the problems China faces by:

- (1) Improving the overall performance of climate system models, enhancing the ability of climate simulations, and further advancing China's international status in climate model research.
- (2) Significantly improving the projection ability with respect to regional-scale climate change, especially trends in extreme climate events.
- (3) Enhancing the ability to mitigate and adapt to climate change by providing scientific support to related international discourse.

1.2 Objectives

1.2.1 General Goals

A high-resolution climate system model with fully coupled atmosphere–ocean–land–ice modules will be established. The model will satisfy the requirements of sustainable development, and be suitable for the climatic characteristics of China, capable of representing the present climate status and projecting future climate change. The model system will be used to study global and East Asian climate change to a similar standard as equivalent international model systems, and will demonstrate better performance in its simulation of the East Asian monsoon. The model will participate in international model comparison projects, promote China's international status in climate system model development and climate change projection, and provide a scientific basis for state planning and decision-making in meteorological disaster prevention and mitigation, climate change, and so on.

1.2.2 Objectives of the 5-Year Project

- (1) Establish a high-resolution global AGCM with a horizontal resolution of approximately 50 km; develop physical parameterization schemes appropriate

- to the high model resolution, and make notable improvements compared to previous models in aspects such as cloud and radiation processes, cloud characteristics, and so on; develop an improved land process model.
- (2) Establish a high-resolution global OGCM with a horizontal resolution of approximately 30–50 km; improve—compared to previous models—the parameterization scheme of vertical mixing; develop an improved sea ice model.
 - (3) Establish a high-resolution climate system model, and notably increase its overall performance compared to previous coupled models; demonstrate distinct advantages in its simulation of East Asian monsoon.
 - (4) Establish observational metrics for evaluating the high-resolution climate system model, and propose methods to recognize and decrease model uncertainty.
 - (5) Participate in international model comparison projects based on research achievements.
 - (6) Foster a team of internationally influential scientists in the field of climate modeling; form a team of early career researchers that make realistic and practical contributions to national demands, and ensure the future sustainable development of the climate system model in China.
 - (7) Publish 50 research papers in top-level journals based on the research achievements.

1.3 Subprojects

The overall project comprises four subprojects (see Table 1.1). The first and second subprojects focus on developing the high-resolution models: the first subproject is entitled *Studies on the High-Resolution AGCM and OGCM* and the research team members mainly come from the IAP, CAS; the second subproject is entitled *Studies on the Resolution and Physical Processes of both Coupled and Uncoupled Models* and the research team members mainly come from the NCC, CMA. The objectives of these two subprojects include:

Table 1.1 The subprojects and their principal investigators (PIs)

	Subproject	PI(s)	Affiliation
1	Studies on the high-resolution AGCM and OGCM	Guangqing Zhou	IAP, CAS
2	Studies on the resolution and physical processes of both coupled and uncoupled models	Rucong Yu and Tongwen Wu	BCC, CMA
3	Development and testing of a multi-model ensemble coupling framework	Wei Xue	Tsinghua University
4	Understanding uncertainties of climate modeling over the East Asian–Western Pacific domain	Tianjun Zhou	IAP, CAS

- (1) Establish a high-resolution AGCM with a horizontal resolution of approximately 50 km; design a dynamic framework with good stability and physical conservation, and apply a coordinated time decomposition algorithm and flexible ease hopscotch scheme to relieve the calculation of disorder and instability in the polar regions; adopt advanced cloud–aerosol–radiation schemes via international cooperation, and make them compatible with the high-resolution model dynamical framework; design a high-resolution OGCM framework with a horizontal resolution of approximately 30–50 km.
- (2) Establish a fully coupled high-resolution climate system model comprising the high-resolution AGCM and OGCM, and the improved sea ice and land process models; improve—compared to previous coupled models—the key physical processes in the coupling procedure, and the performance of the model in the following aspects: cloud microphysics (including the development of a cloud-precipitation physical scheme suitable for the East Asian climate); cloud–radiation interaction; vertical mixing; atmospheric boundary layer; and land process parameterization.

The third subproject is entitled *Development and Testing of a Multi-model Ensemble Coupling Framework*. The team members are from Tsinghua University and the NCC, CMA, with the former being computer science experts and the latter specializing in climate modeling and projection. The scientists from these two communities work together to investigate the ocean–atmosphere coupling multi-flux ensemble method, optimize the atmosphere flux forcing on the ocean, and reduce the simulation biases caused by air–sea flux uncertainty, thereby improving the performance of the climate system model.

The fourth subproject is entitled *Understanding Uncertainties of Climate Modeling over the East Asian–Western Pacific Domain*. The team members are mainly from the State Key Laboratory of Numerical Modeling for Atmospheric Sciences and Geophysical Fluid Dynamics (LASG)/IAP, CAS. The task of the subproject is to comprehensively evaluate the performance of the high-resolution climate system model with a focus on the East Asian–Western Pacific climate. It is hoped that the team will establish solid observational metrics for gauging model performance over East Asia, and identify the potential added value of the high-resolution model in reducing the biases in the tropics and in the simulation of energy transport. The sensitivity of the climate system model to greenhouse gas forcing, and the physical processes that affect model sensitivity will also be investigated. One particular task of this subproject is to assess the strengths and weaknesses of high-resolution models in simulating Asian–Australia monsoon (including the East Asian monsoon). In addition, the team is also responsible for developing an interdecadal climate prediction system and carrying out near-term climate change projection experiments designed by the Coupled Model Intercomparison Project Phase 5 (CMIP5) for the Fifth Assessment Report of the Intergovernmental Panel on Climate Change (IPCC AR5), and studying the potential change in future East Asian monsoon.

1.4 Overview of the Project Implementation

After 5 years of research and development, the following achievements have been made:

- (1) A fully coupled high-resolution climate system model (BCC_CSM2.0) has been established. The horizontal resolution of the AGCM is T266 (approximately 45×45 km) and the horizontal resolution of the OCGM is 30 km in the tropics. Both the dynamic core and the physical parameterization of the AGCM have been improved compared to previous models. BCC_CSM2.0 shows reasonable performance in reproducing regional climate features and Asian summer monsoon in comparison to its low-resolution (280×280 km) counterpart.
- (2) The IAP AGCM4.0, with a horizontal resolution of $0.5^\circ \times 0.5^\circ$, has been developed based on the previous version with resolution $1.4^\circ \times 1.4^\circ$. Several new methods, such as a flexible leaping-point scheme, time-splitting methods, and a 2D parallel algorithm, have been introduced into the dynamical core to make the high-resolution model more efficient and stable. Thirty-year (1979–2008) integrations of the Atmospheric Model Intercomparison Project (AMIP) run with the model have been completed. The simulated seasonal migration of the rain belt over the East Asian monsoon area is better than that in the coarse-resolution model compared with Global Precipitation Climatology Project (GPCP) data. The sensitivity of the simulated climate to different dynamical cores has also been investigated. For the physical parameterizations, the interactive Cloud–Aerosol–Radiation ensemble model (CAR system) has been fully evaluated and incorporated into the CAS climate system model (IAP AGCM4), and numerical simulations by selecting some of the parameterizations in the CAR system are in progress.
- (3) The ensemble method is effective at reducing model uncertainties. Supported by the project, a novel ensemble technology has been developed and employed to the coupling process in the climate system model, forming a flexible multi-model ensemble coupling platform. This platform can perform the couple of the ensemble of multiple atmospheric models or multiple realizations of one atmospheric model with the ocean model, land model, and sea ice model in single experiment, which enables the quantification study on the role of atmospheric noise and model uncertainty in coupled model. Multiple initial condition ensemble simulations show that stochastic noise generated by atmospheric dynamics is reduced and can be used to estimate the impact of atmospheric perturbations on the ocean and to identify the impact of atmospheric noise in complex sea–air coupling process; better reproduction of the relationship between ENSO and middle–high latitude SST in the North Pacific can be achieved compared to the original standard coupled model.
- (4) Observational metrics for gauging model performance over the East Asian–Western Pacific domain have been developed and applied to CMIP5 models. The proposed metrics focus on the East Asian summer monsoon, ranging in

scale from the diurnal cycle to the intraseasonal, interannual, and interdecadal variability, and also the East Asian cloud and radiation distribution. Additionally, this subproject has extended the application of the metrics from East Asia to the tropical Pacific and examined the processes responsible for the tropical bias. The performances of current state-of-the-art climate models in simulating the monsoon–ENSO relationship have also been assessed, and some suggestions provided on how to improve the simulation of ENSO. The evaluations of CMIP5, BCC, and IAP models using these observational metrics are expected to provide useful references for identifying the added value of high-resolution models over their low-resolution counterparts.

1.5 Major Achievements

1.5.1 *Development of a High-Resolution Version of the BCC_CSM Global Climate System Model*

1.5.1.1 Development of High-Resolution Global AGCMs

Global Spectral AGCM

BCC_AGCM3.0 is a newly developed high-resolution AGCM. The model dynamics of BCC_AGCM3.0 is the same as the spectral framework of its predecessors BCC_AGCM2.0, BCC_AGCM2.1, and BCC_AGCM2.2 (Wu et al. 2008, 2010b, 2014), but with a global horizontal resolution of T266 (0.45° latitude \times 0.45° longitude) and 26 vertical layers.

BCC_AGCM2.0 is the first version of the second generation of AGCMs developed by the BCC (Beijing Climate Center). It is a global spectral model with a horizontal resolution of T42 (approximately $2.8125^\circ \times 2.8125^\circ$ on a transformed grid) and 26 levels in a hybrid sigma/pressure vertical coordinate system with the top level at 2.914 hPa. The dynamical core of the model is described in Wu et al. (2008), and a previous version (BCC_AGCM2.0) is detailed in Wu et al. (2010b). Most of the physical processes are from version 3 of the Community Atmosphere Model (CAM3) developed by the National Center for Atmospheric Research (NCAR). A few new schemes are implemented, including parameterizations for deep cumulus convection, dry adiabatic adjustment, latent heat and sensible heat fluxes over the ocean surface, and snow cover fraction (Wu et al. 2010b). BCC_AGCM2.1 and BCC_AGCM2.2 are updated versions of BCC_AGCM2.0 with a new deep penetrative convection scheme suggested by Wu (2012), but with T42 and T106 horizontal resolutions, respectively. Additionally, there is the option for atmospheric CO₂ concentration to be simulated under the forcing of anthropogenic carbon emissions.

Further improvements have been made in BCC_AGCM3.0, including:

- (1) An enhanced model dynamics framework suitable for high-resolution modeling. In addition to the original semi-Lagrangian advection transport scheme, a two-step shape-preserving advection scheme (TSPAS) (Yu 1994) and a flux-form semi-Lagrangian (FFSL) transport scheme are available for optional use.
- (2) In previous BCC_AGCM versions, the parameterization for gravity wave drag only involves the gravity waves generated by orography. In BCC_AGCM3.0, gravity waves generated by all major sources—including convection and geostrophic adjustment—are involved.
- (3) The parameterization scheme for mass-flux-type cumulus convection developed by Wu (2012) has been improved. It is a simple mass-flux cumulus parameterization scheme suitable for large-scale atmospheric models. The scheme is based on a bulk-cloud approach with its own unique properties, especially for the treatment of convective updrafts and downdrafts (Wu 2012).
- (4) Humidity-based cloud fraction parameterization has been improved, and there is an option to use a statistical cloudiness parameterization scheme based on the probability density function (PDF) of cloud water.
- (5) A new scheme for sensible and latent heat fluxes from the ocean surface, based on the work of Wu et al. (2010a), has been implemented. The stability functions, roughness lengths, and sea spray effects to parameterize the surface turbulent fluxes between air and sea are involved.
- (6) The land surface process scheme has been updated from BCC_AVIM1.0 to BCC_AVIM2.0.
- (7) A global-gridded AGCM version has been developed to explore the different performances of the high-resolution models.

Global-Gridded AGCM

Version 4 of the IAP AGCM (IAP AGCM4.0) with a high resolution of $0.5^\circ \times 0.5^\circ$ has been developed based on a previous version with resolution $1.4^\circ \times 1.4^\circ$, which itself evolved from several other earlier versions (Zeng et al. 1989; Liang 1996; Zuo 2003; Zhang et al. 2013c). Several new methods, such as a flexible leaping-point scheme, time-splitting methods, and a 2D parallel algorithm, have been introduced into the dynamical core to make the high-resolution version more efficient and stable (Zhang 2009). When the flexible leaping-point scheme is used, the time-step increases to three times the original because of the threefold larger zonal grid size, thus saving computing time. The time-splitting method is used to split the model equations to integrate the advection terms with large time-step and the inertia-gravity wave terms with small time-step, which also saves computing time. The model can integrate 8 months/day on 1024 processing cores using the new 2D parallel algorithm, and the parallel efficiency is about 20 %.

Thirty-year (1979–2008) integrations of the AMIP run with this high-resolution model have been completed, and preliminary evaluations suggest that the simulated

zonal mean and global distribution of precipitation and sea level pressure are in good agreement with observations. The seasonal migration of the rain belt over the East Asian monsoon area simulated using the high-resolution model is better than that with the coarse-resolution model, as judged by comparisons with GPCP data.

The sensitivity of the simulated climate to different dynamical cores has also been investigated. The tropospheric temperature in the IAP model with full physics is colder than that in CAM3.1 at low and midlatitudes. However, when the dynamical core is used in dry simulation, the IAP model simulates a warmer troposphere than CAM3.1. The IAP dynamical core also simulates weaker eddies in both the full physics and dry simulations than those in CAM due to different numerical approximations. Our interpretation of these differences between dry and moist simulations is that, in dry simulations, the less energetic eddies correspond to less heat transport to the polar regions, which leads to the warmer troposphere in the IAP model. In moist simulations, however, the less energetic eddies also cause less upward transport of water vapor and less high-cloud amount in the IAP model. The reduced high-cloud amount corresponds to increased radiative cooling of the atmosphere in the IAP model, leading to a colder troposphere relative to CAM3.1.

Radiative Transfer Uncertainty

In physical parameterizations, radiative processes are fundamental, playing central roles in many proposed climate change mechanisms. The uncertainty in radiative transfer calculations represents an important limitation for progress in climate modeling. The need for accurate radiative transfer calculations, especially under cloudy and aerosol-laden conditions, has been emphasized (IPCC 2013). In particular, under partly cloudy skies, quite large inconsistencies among models appear due to the commonly used, unnatural coupling between assumptions about cloud vertical overlap and methods for computing radiative transfer. The role of unresolved cloud structures in the different estimated irradiances and cloud radiative effects of current models is far from understood, which limits agreement among studies on cloud/aerosol/radiation interactions and feedback.

Two advanced methods are now available for explicit representation of cloud subgrid-scale structures in 1D radiation codes: the mosaic method (Liang and Wang 1997) and the Monte Carlo Independent Column Approximation (McICA) (Barker et al. 2002; Pincus et al. 2003; Räisänen et al. 2004). Recently, both approaches have been successfully incorporated into the CAR system, along with seven radiative transfer schemes commonly used at major climate prediction centers worldwide (Liang and Zhang 2013; Zhang et al. 2013a). It is the first time that we have consistently realized the decoupling of the assumption of cloud subgrid-scale structures from the calculation of radiative transfer for multiple radiation transfer codes in a unified system. Such decoupling not only allows for more flexible, complex, and realistic cloud descriptions, but also simplifies the radiative transfer algorithms. In addition, the CAR system incorporates those cloud, aerosol, and radiation parameterizations commonly used by current climate/weather models at

key operational centers and research institutions worldwide. Based on its modular design, all built-in cloud methods, including mosaic and McICA, and aerosol parameterizations are fully compatible with, and hence can be selected and fully exchanged with, all major radiation transfer schemes in the CAR system. Therefore, the CAR system has the unique ability to allow more rigorous evaluation of different cloud/aerosol/radiation schemes and ultimately improve understanding of cloud–aerosol–radiation interactions and feedbacks in climate studies.

Recently, through international cooperation, the CAR system has been fully evaluated, and some interesting results about the large spread of current radiative calculations are obtained (Zhang et al. 2013a, b). The CAR system has been incorporated into the CAS climate system model (IAP AGCM4), and numerical simulations involving various parameterization selections in the CAR system are in progress.

We have conducted a full evaluation of the overall accuracy and efficiency of the CAR system among a suite of alternative schemes that are frequently used in GCMs and regional climate models. Two different sets of experiments have been conducted: CIRC experiments, in which Continuous Intercomparison of Radiation Codes (CIRC) Phase I cloudy case data (cases 6 and 7) are used to drive the CAR system; and ERI experiments, in which 6-hourly ERA-Interim observational analysis data (ERI) for January and July 2004 are used to drive the CAR system. In the ERI experiments, there are three subsets of experiments for (1) evaluating the overall accuracy of the original radiation transfer codes, (2) evaluating the overall accuracy of the CAR system, and (3) evaluating the effects of cloud subgrid structures. These evaluations offer a basic assessment of the CAR system’s modeling accuracies. Given the range of the best available observations, the CAR ensemble means for top of the atmosphere (TOA) and (surface) SFC radiative fluxes achieve very reasonable accuracies. Additionally, the model spreads in July completely cover the observational ranges, with ensemble means located in the centers, indicating a successful and robust implementation of the CAR system. This establishes the credibility of the CAR system and encourages its broad application in climate studies in the future. In addition, quite large uncertainty ranges are found for cloud radiative forcings (or effects), implying that these model spreads are mainly caused by the different treatments of unresolved cloud structures, cover fractions, top-level positions, particle effective size, and optical properties. The calculation accuracies of the original radiation transfer codes can be enhanced using different cloud schemes, including those for cloud cover fraction, particle effective size, water path, and optical properties, and using better treatments, such as the MOSAIC or McICA method, for unresolved cloud structures that can explicitly treat the effects of cloud subgrid variability.

Using the CAR system, we have also quantified the spread of radiation transfer calculations among different cloud/radiation scheme combinations. Among 448 selected CAR members (i.e., 7 major radiation transfer schemes \times 64 cloud schemes; Liang and Zhang 2013; Zhang et al. 2013a), there is a substantial spread of 30–60 W m⁻² in TOA/SFC longwave/shortwave all-sky fluxes, as well as in TOA/SFC cloud radiative forcings (effects). The large inter-model discrepancies in

cloud radiative forcings primarily come from different cloud treatments that were originally adopted by different radiation codes. For July, the model spreads completely cover the observational ranges, with ensemble means located in the centers of such ranges. This indicates a reasonable performance of the CAR system, with very good accuracies of the CAR ensembles. It has also been noted that, for January, almost all observations fall at the tails of the model distributions, which infers the possibility that the cloud/radiation representations in winter are not properly parameterized, the schemes chosen are not varied enough, or the ERI cloud water fields are poor quality. In addition, the best available observational estimates (i.e., Clouds and the Earth's Radiant Energy System (CERES), CERES Energy Balanced and Filled (CERES_EBAF), International Satellite Cloud Climatology Project (ISCCP), and Surface Radiation Budget (SRB)) also contain nontrivial uncertainties, ranging from 5 to 15 W m^{-2} on a global basis.

Using the CAR system, we conducted a study on the key factors of model differences in cloud radiative effects (CREs) among the seven radiation codes commonly used at the major climate prediction centers worldwide. It was the first time that we had quantitatively investigated why large model discrepancies in estimated cloud radiative forcings and irradiances exist among current 1D radiation transfer codes aimed at climate studies. In the study, several sets of numerical experiments were performed to elucidate each individual contribution of each scheme's diversity in cloud optical properties, cloud horizontal variability, cloud vertical overlap, and gas absorption. These global experiments were driven by 6-hourly ERI observational analysis data for July 2004. Each set had 98 global runs, combining 14 cloud cover members and 7 radiative transfer schemes. After removing most of the disagreement in the cloud fields, the model spread of CREs among the CAR system's seven major radiation schemes, as well as that of radiative flux, dramatically diminished. Taking global mean CREs as an example, based on the same 3D distributions of cloud condensates and cover fractions, the model ranges decreased to $<4 \text{ W m}^{-2}$ from about 10 W m^{-2} for shortwave radiative flux and $5\text{--}8 \text{ W m}^{-2}$ for longwave radiative flux when using similar cloud fields among the different radiation schemes. Generally, subgrid-scale cloud structures (including vertical overlap and horizontal variability) played dominant roles, explaining about 40–75 % of the total model spread.

The complicated nonlinearity of the coupling of cloud/radiation processes was highlighted in the study. Inter-model variation among the different radiation codes varied strongly with different cloud cover members (clds.), and both the existing inter-cld. discrepancies (i.e., discrepancies among different clds.) and inter-cop discrepancies (i.e., discrepancies among different cloud optical property members) were also dependent on the radiation transfer code. The major reasons were investigated. In general, using different assumptions of cloud vertical overlap accounted for most of the sensitivity in the inter-model diversity to different clds. Different clds. produced different vertical profiles of cloud cover fraction, which determined whether and to what extent the different assumptions of cloud vertical overlap mattered for the radiation. The different ranges of clear-sky portions among the different radiation codes then generated the large nonlinear sensitivity to

different clds. By removing the contributions from the different treatments of the key cloud factors, the remaining nonlinear effects between cloud and radiation were largely reduced. Hence, we confirmed the importance of the CAR system to our studies on cloud/aerosol/radiation processes, and therefore on climate change projections as well.

Moreover, given the existing large inter-model diversity, only a specific group of methods can be used to improve the performances of the different radiation codes. These methods are model dependent, i.e., they work well for some radiation codes but may not work well for others. This largely obscures the roles of cloud in radiation transfer. However, using a system like the CAR, we now have the ability to significantly diminish the model discrepancies. Consequently, more evaluations of radiation transfer codes can be carried out to consistently improve cloud water fields, cloud optical property schemes, and/or treatments of cloud subgrid-scale structures. For example, as shown in our study, after removing most of the disagreement in the cloud fields, and through combination with *cop1* (i.e., cloud optical property member 1), the McICA method with a generalized overlap generator produced better modeled CREs and irradiances for most cloud cover members than with a maximum-random overlap generator. The CAR provides a more realistic approach to search for an optimal model, and would enhance our physical understanding of cloud and radiation processes and their interaction and feedback in climate models.

1.5.1.2 Development of High-Resolution Global OGCMs

MOM4_L40 is a global OGCM and a very important component of the high-resolution climate system model BCC_CSM2.0. It was based on MOM4, developed by the Geophysical Fluid Dynamics Laboratory (GFDL) and has the following features (Wu et al. 2014): It uses a global three-pole grid, in which the North Pole is imposed on both North America and the Eurasian continent. Its horizontal resolution is 1° longitude \times 1° latitude beyond 30°N and 30°S , incrementally descending to the equator by $1/3^\circ$ latitude within 30°N and 30°S . The model has 40 vertical layers, with the top 200 m divided into 20 equal-thickness 10-m layers. The main physical parameterization schemes (Griffies et al. 2005) include Sweby's (1984) tracer-based third-order advection, the isopycnic surface mixed tracer diffusion scheme of Gent and McWilliams (1990), a Laplace horizontal friction scheme, the K-profile parameterization mixed-layer scheme of Large et al. (1994), complete convective adjustment, and sea floor boundary/steep topography overflow processing, allowing unstable gravity-driven fluid elements to flow down slope in the upstream advection scheme. The effects of the spatial distribution of chlorophyll are also taken into account in calculating the shortwave solar irradiance penetration (Sweeney et al. 2005). To simulate the ocean carbon cycle, MOM4_L40 incorporates the ocean carbon cycle module from MOM4 FMS, a module that was based on the Ocean Carbon Model Intercomparison Project Phase 2 (OCMIP2). There are two versions of MOM4_L40, which have different land and submarine topographies:

MOM4_L40v1 uses the ocean component from BCC_CSM1.1, while MOM4_L40v2 uses that of BCC_CSM1.1(m). The oceanic component of BCC_CSM2.0 is MOM_L40v2, and the main developments are: (1) a parameterization scheme for vertical mixing due to inertial internal wave breaking, and (2) the inclusion of nonbreaking-wave-induced vertical mixing processes. A higher resolution version of the ocean model (MOM4_L50) is under development. MOM4_L50 has a horizontal resolution of 1° – $1/6^{\circ}$ (from poles to equator) in latitude and 0.5° in longitude, with 50 vertical layers. The fundamental framework and schemes of MOM4_L50 are the same as in MOM4_L40.

Based on the Hybrid Coordinate Ocean Model (HYCOM; Bleck 2002), a global ocean model with a resolution of 7–30 km has been developed. The model includes a sea ice model and the effects of freshwater flux from 922 rivers. There are 30 layers in the vertical direction using a hybrid system of z -level, terrain-following (sigma), and isopycnic coordinates. Two experiments in which two different reference densities for the vertical coordinate are, respectively, set at the surface (EXP_SFC) and at a depth of 2000 m (EXP_2000) are underway. Only 42-year integrations of the two experiments have been completed thus far, and the model is still in its adjustment phase to reach equilibrium, especially in the deep ocean. Nevertheless, preliminary results show that, in both experiments, the model basically reproduces the main circulation features of the global ocean. EXP_SFC simulates the circulation at the ocean surface better than EXP_2000, while EXP_2000 simulates the circulation in the mid and deep ocean better than EXP_SFC. However, some discrepancies are apparent. Sensitivity experiments show that the selection and setting of vertical coordinates in the model greatly affect the simulation results. For example, to reproduce a better thermocline structure and undercurrent system in the tropical Pacific, the z -coordinate throughout the entire thermocline depth of about 200 m from the surface is a good choice. Much more work on tuning the model is necessary.

1.5.1.3 Development of the High-Resolution Land Component Model

BCC_AVIM2.0 is the newly developed version 2 of the BCC's Atmosphere–Vegetation Interaction Model, and is suitable for inclusion in BCC_CSM2. Its previous version, BCC_AVIM1.0, was developed on the basis of version 3 of the NCAR's Community Land Model (CLM3.0) and AVIM2, and includes: (1) A soil moisture and heat transfer module similar to that of CLM3.0, with its underlying surfaces falling into four categories: soil, wetland, lake, and glacier. The soil is vertically divided into ten layers, plus one vegetation layer, with snow cover partitioned up to five layers depending on the snow depth. The land vegetation is divided into 15 plant functional types (PFTs), and each model grid box includes up to four PFTs (Oleson et al. 2004). (2) A module that incorporates vegetation dynamics and soil carbon decomposition processes from AVIM2 (Ji 1995; Ji et al. 2008). The module describes the terrestrial carbon cycle, including CO_2 sequestration through photosynthesis, vegetation growth, and dieback, and CO_2 release

back into the atmosphere through soil respiration. (3) A revised snow cover parameterization scheme, which takes into account multiple factors (e.g., snow depth, surface roughness, subgrid topography) for the snow cover fraction (SCF), which is generally underestimated in CLM3.0, to improve the positive bias in SCF simulations in regions with rough topography, such as the Tibetan and Mongolian plateaus.

Several improvements have been made in BCC_AVIM2.0:

- (1) The temperature threshold for soil freezing has been modified. The method for calculating the critical freeze–thaw temperature in soil used by Li and Sun (2007) has been adopted to replace the unreasonable assumption used in CLM3.0.
- (2) On the basis of previous research, a new parameterization scheme has been developed to consider the influences of these materials on soil thermal and hydrological conductivities (Ma et al. 2014).
- (3) In many parameterizations for snow albedo, the snow surface temperature is considered the most important, and sometimes the only, factor involved. In BCC_AVIM2.0, several physical parameters such as air temperature, the temperature difference between the air and snow surface, wind speed, and other factors that affect the growth rate of snow grain size and ultimately influence snow albedo, are taken into account.
- (4) The function of the temperature adjustment to the maximum rate of carboxylation of vegetation photosynthesis has been modified. Its dependence on PFT is considered. This consideration is more reasonable for vegetation photosynthesis.
- (5) To achieve a more accurate representation of canopy albedo, a four-stream radiative transfer model within the canopy is used in place of the original two-stream radiative transfer model.

1.5.1.4 Development of BCC_CSM

Under the support of the present project, a high-resolution climate system model (BCC_CSM2.0) has been established. It is a fully coupled atmosphere–ocean climate system model with a horizontal resolution of T266 (approximately 45×45 km) in the atmosphere and 30 km in the tropical ocean. Its development is based on a lower resolution version (BCC_CSM1.1; Wu et al. 2013) [T42 (approximately 280×280 km)], over which many improvements to the dynamic framework and model physics parameterizations have been made. The atmospheric component is an updated version (version 3.0) of version 2.1 of the BCC’s Atmospheric General Model (BCC_AGCM2.1). BCC_AGCM2.1 has a resolution of T106, whereas BCC_AGCM3.0 has a resolution of T266. The land component has been updated from BCC_AVIM1 to BCC_AVIM2. The ocean component is MOM4_L40, and its horizontal resolution is 1° longitude by $1/3^\circ$ latitude between 30°S and 30°N ranged to 1° latitude at 60°S and 60°N and nominally 1° polarward

with tripolar coordinates to resolve the arctic. The sea ice component is the sea ice simulator (SIS), which has the same horizontal resolution as MOM4_L40. All four components are fully coupled via a flux coupler.

All the improvements made in BCC_CSM2.0 to the dynamic framework and model physics have been described in Sect. 1.5.1. Its stability in long-term runs has been tested. To initialize the coupled simulations, each component of BCC_CSM performed individual “spin-up” runs to generate equilibrium initial conditions. Then, BCC_CSM was run for a historical simulation for 50 years from 1958 to 2007, with external forcing changes through time that included well-mixed greenhouse gases, ozone, aerosols, solar radiation, and volcanoes. The time evolution of global mean SST indicated that BCC_CSM had reached a quasi-steady state. The results show that the high-resolution model (i.e., BCC_CSM2.0) performs better than its lower resolution predecessors, especially in the following aspects:

- (1) *Global precipitation distribution.* The high-resolution model can reasonably reproduce the general distribution of precipitation over the globe, demonstrating clear improvement in the northern tropical maximum, southern tropical second peak, and precipitation over the middle to high latitudes of the Northern Hemisphere. Furthermore, BCC_CSM2.0 can reasonably reproduce the major characteristics of the spatial distribution of June–August mean precipitation over the globe.
- (2) *Regional temperature over East Asia.* Comparatively, the high-resolution model produces better simulations of temperature at the regional scale, such as in the Sichuan Basin, Northeast China, and West China. The warm center around the Sichuan Basin—omitted in lower resolution models—is reproduced well. The regional distribution of temperature in Northeast China is more consistent with observations than lower resolution models. The particular distribution of temperature in the provinces of Xinjiang and Xizang can only be captured by the high-resolution model.
- (3) *East Asian summer monsoon.* The East Asian monsoon precipitation is characterized by a stepwise meridional evolution. All versions of BCC_CSM simulate the main south–north movement of the rain belt with time, but the increased horizontal resolution in the latest version may be partly responsible for the improved capability in representing the annual cycle of rainfall over East Asia. The intensity of maximum rainfall occurs in the so-called East Asian Summer Monsoon (EASM) period, and is best captured by BCC_CSM2.0. The timings of the Asian-Pacific monsoon onset, peak, and withdrawal show some improvements in BCC_CSM2.0 compared to BCC_CSM1.1 and BCC_CSM1.1 m, and BCC_CSM2.0 is best at simulating the monsoon duration.
- (4) *SST over the tropical Pacific Ocean.* The simulated characteristics of the annual cycle, peak phase, and westward propagation of equatorial Pacific SST are improved in BCC_CSM2.0. Compared to the lower resolution versions, the simulated annual cycle of SST in BCC_CSM2.0 is closer to that of

HadISST data (Rayner et al. 2003). It is clear from simulations of the three versions of BCC_CSM that increasing the horizontal resolution has improved the simulated meridional asymmetry in the tropical Pacific. This improvement is due to the more reasonable representation of ocean–atmosphere interaction. Another improvement in BCC_CSM2.0 is the teleconnection spatial pattern between El Niño and global SST. The teleconnection distribution in BCC_CSM2.0 is reasonable, and the main areas of positive and negative correlation are close to HadISST observations.

1.5.2 The Model Evaluation System

Supported by the project, a set of comprehensive metrics that can be used to evaluate model performances over the East Asian–Western Pacific region has been established. The evaluation system consists of four parts: (1) metrics for East Asian summer monsoon, including the diurnal cycle, mean states, intraseasonal variation, interannual variability, interdecadal variability, and its global monsoon context; (2) metrics for East Asian cloud and radiation, including stratus cloud over East Asia, the divergence and stability of the atmosphere downstream of the Tibetan Plateau, and cloud radiation budgets; (3) metrics for the tropical climate and tropical bias in coupled models; and (4) metrics for simulations of ENSO and ENSO–monsoon interaction. The details of these metrics are described in Chap. 5. However, the performances of CAM5, BCC_CSM, and CMIP5 models based on some of these metrics have been analyzed, and the results are reported, in this section. Both CAM5 and BCC_CSM have three resolutions, i.e., T42, T106, and T266.

1.5.2.1 Metrics for EASM

In the observation (Fig. 1.1a), the summer climatological circulation over the East Asian–Western Pacific is characterized by the western edge of the western North Pacific subtropical high (WNPSH). On the western flank of the WNPSH, southerly wind prevails over eastern China. These features are captured by the multi-model ensemble (MME) of CMIP5-AMIP models (Fig. 1.1b). The difference in the 850 hPa wind between the CMIP5 MME and the observation is characterized by a cyclonic anomaly over the southern WNP centered at about 20°N, and an anticyclonic anomaly over the northern WNP centered at about 40°N, suggesting a northward displacement of the ridge of the WNPSH (He et al. 2014). The difference in the precipitation between the CMIP5 MME and the observation is characterized by excessive rainfall over the southern WNP and deficient rainfall over the northern WNP, consistent with the circulation bias.

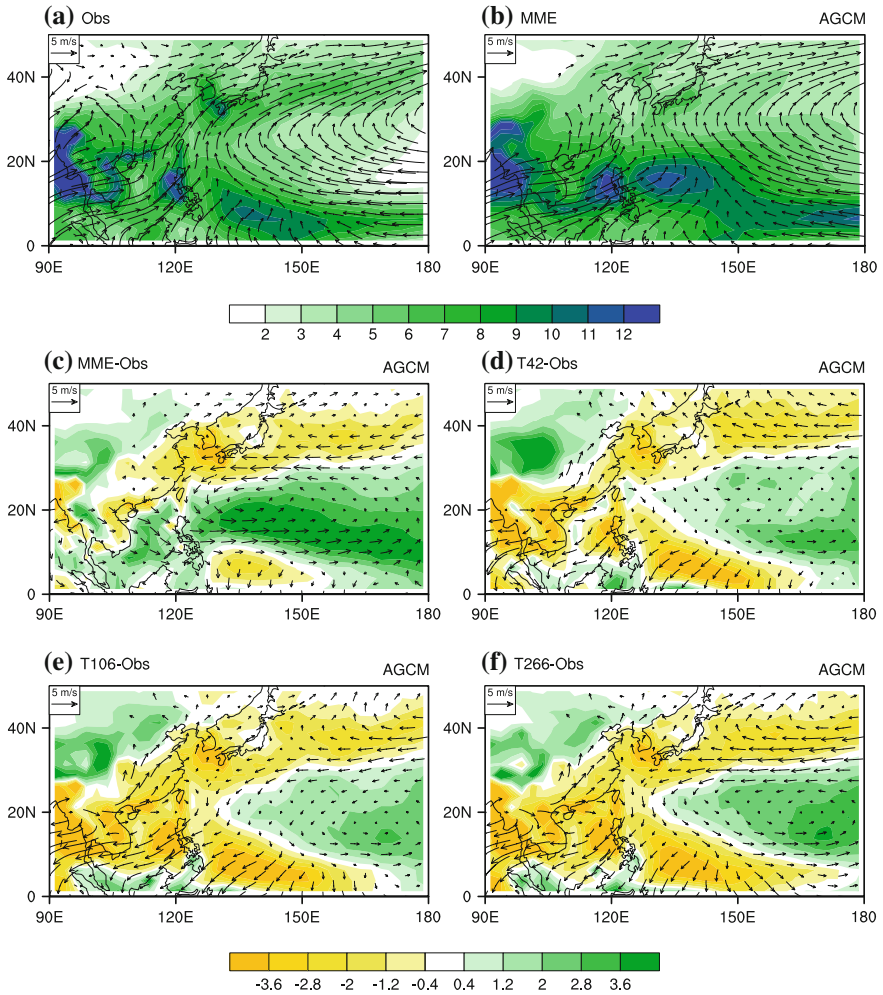


Fig. 1.1 **a** Summer mean state of precipitation (units: mm day^{-1}) and wind at 850 hPa (units: m s^{-1}) in the observation. The wind field is from the NCEP2 data (Kanamitsu et al. 2002) and precipitation field is from the GPCP data (Adler et al. 2003). **b** Multi-model ensemble (MME) simulated mean state of precipitation and wind at 850 hPa in AGCMs of CMIP5. **c-f** Difference in the mean state of precipitation and 850 hPa wind between simulations and observation: **c** MME; **d-f** T42, T106, and T266 resolutions of CAM5, respectively

Similar to the CMIP5 MME, the difference between CAM5 and the observation is also characterized by a cyclonic anomaly over the southern WNP and an anti-cyclonic anomaly over the northern WNP, accompanied by excessive rainfall over the southern WNP and deficient rainfall over the northern WNP (Fig. 1.1d-f). These biases are common for the T42, T106, and T266 resolutions, suggesting that over the WNP they are not sensitive to the horizontal resolution. A comparison

between the three resolutions of CAM5 shows that the excessive rainfall on the eastern flank of the Tibetan Plateau is reduced as the horizontal resolution increasing (Fig. 1.1d–f), suggesting that the simulation of precipitation on the lee side of the Tibetan Plateau can be improved by a better description of the topography (also see Li et al. 2015).

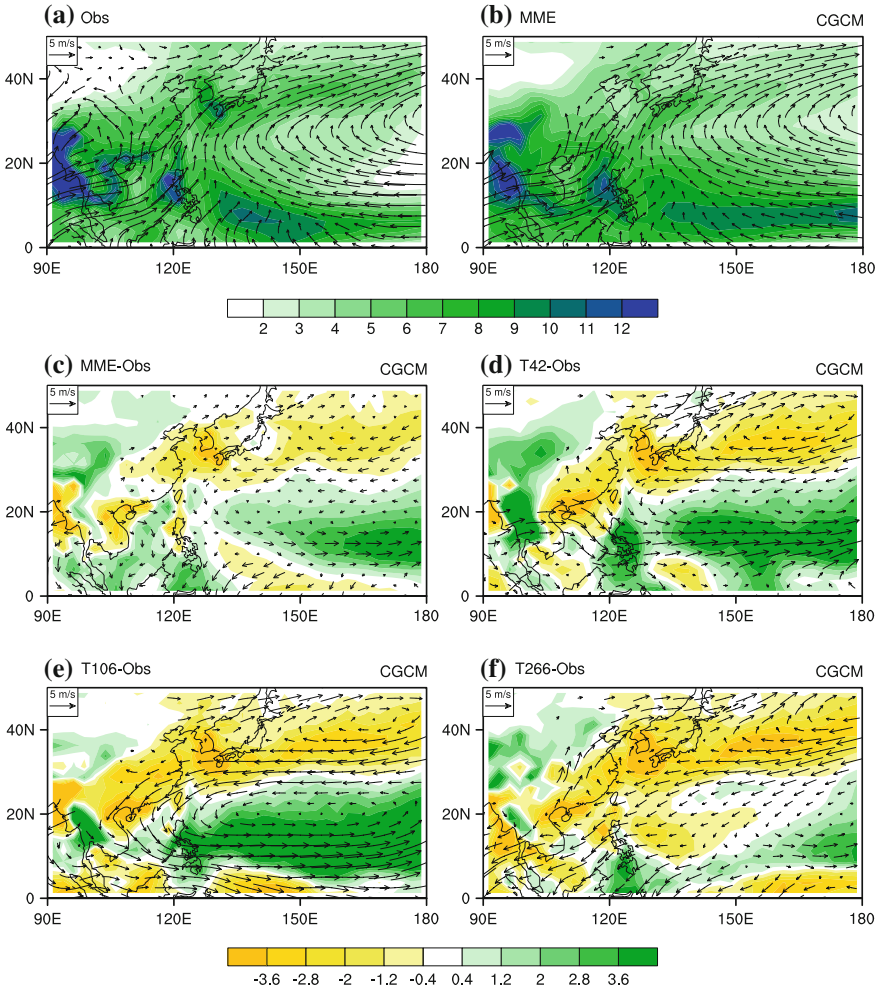


Fig. 1.2 **a** Summer mean state of precipitation (units: mm day⁻¹) and wind at 850 hPa (units: m s⁻¹) in the observation (NCEP2 data for the wind field and GPCP data for the precipitation field). **b** Multi-model ensemble (MME) simulated mean state of precipitation and wind at 850 hPa in CGCMs of CMIP5. **c–f** Difference in the mean state of precipitation and 850 hPa wind between simulations and observation: **c** MME; **d–f** T42, T106, and T266 resolutions of BCC_CSM, respectively

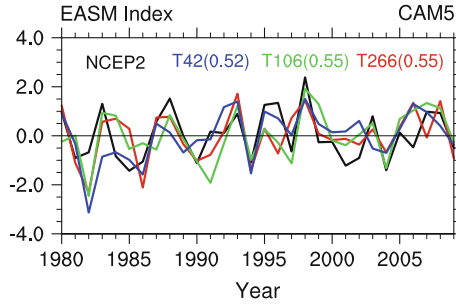


Fig. 1.3 Temporal evolution of the standardized EASM index in NCEP2 (*black line*), AMIP experiment from CAM5 T42 (*blue line*), T106 (*green line*), and T266 (*red line*) during 1980–2009. The numbers in brackets are the correlation coefficients with the observation

The observed mean state is also captured by the MME of the historical simulation of the CMIP5 models (Fig. 1.2b). Similar to the AMIP simulation, the bias in the mean state of the coupled models is also characterized by excessive rainfall and a cyclonic anomaly over the southern WNP, and deficient rainfall and an anticyclonic anomaly over the northern WNP (Fig. 1.2c), but with weaker magnitude than the CMIP5-AMIP models.

The precipitation on the eastern side of the Tibetan Plateau improves as the horizontal resolution increases in BCC_CSM (Fig. 1.2d–f), as does the mean state over the southern WNP. In the T42 and T106 versions of BCC_CSM, the southern WNP is characterized by an anomalous cyclone and excessive rainfall compared with the observation (Fig. 1.2d, e). It is encouraging that in the T266 version of BCC_CSM this bias has almost vanished (Fig. 1.2f).

To investigate the possible impact of the horizontal resolution on the interannual variability of the EASM, three AMIP experiments from different resolutions of CAM5 are compared (Figs. 1.3 and 1.4). To measure the strength of the EASM, the monsoon circulation index defined as the wind shear along the western flank of the WPSH (Song and Zhou 2014a, b) is used. All three versions of CAM5 can capture well the observed evolution of the EASM. The correlation coefficients between the observation and the three versions are almost the same (0.52, 0.55, and 0.55) and are all statistically significant at the 1 % level.

To compare the interannual patterns of the EASM simulated by different CAM5 versions, the precipitation and 850 hPa wind are regressed on the observed EASM index (Fig. 1.4). The observed Western Pacific anticyclone (WPAC) and dipole rainfall pattern are captured well in CAM5 T42, although their magnitudes are smaller than observed and the dipole rainfall pattern is shifted southward. With increasing horizontal resolution, the magnitudes of the WPAC and dipole rainfall pattern become smaller. In CAM5 T266, the rainfall pattern is not well organized and is significantly different from the other two CAM5 models. Hence, an influence of horizontal resolution on the large-scale features of the interannual variability of the EASM is not evident.

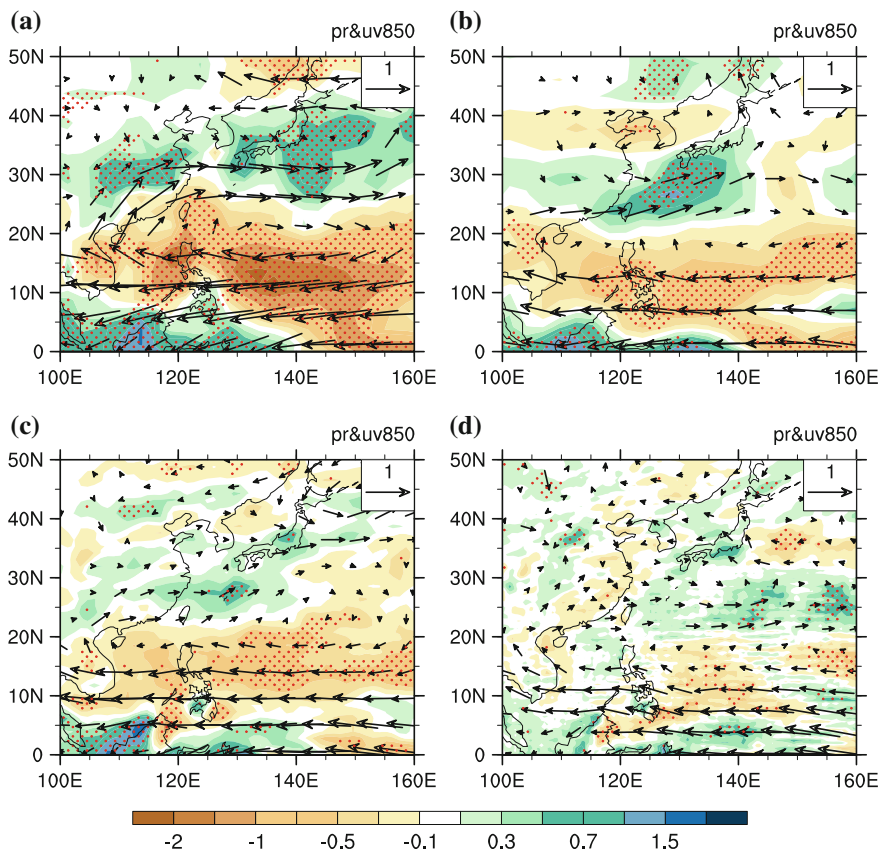


Fig. 1.4 Horizontal distribution of precipitation (shaded; units: mm day^{-1}) and 850 hPa wind (vectors; units: m s^{-1}) regressed on the NCEP2 EASM index during 1980–2009 in **a** GPCP and NCEP2, and the AMIP experiment from **b** CAM5 T42, **c** CAM5 T106, and **d** CAM5 T266. *Red dots* indicate that the regressed precipitation is significant at the 10 % level by the Student's *t*-test

Next, we extend our analysis from East Asia to the global monsoon system. Following the definition of the global monsoon domain proposed by Wang and Ding (2008), followed by Zhou et al. (2008a, b, 2014), the distribution of the annual range of precipitation and the monsoon domain are obtained and shown in Fig. 1.5. In the observation, the monsoon regions are the Asian–Australian monsoon, the North and South African monsoon, and the North and South American monsoon. The CMIP5 MME reproduces well the main monsoon regions, but with unrealistic monsoon over the southern Pacific Ocean along South America coast. Furthermore, the Northwestern Pacific (NWP) monsoon region extends more east than in the observation. In BCC_CSM, the above-mentioned biases exist in the T42 and T106 versions (Fig. 1.5c, d), but not in the highest resolution version (Fig. 1.5e). This difference suggests that the higher resolution model can perform better than the lower resolution models by suppressing the excessive rainfall over the NWP

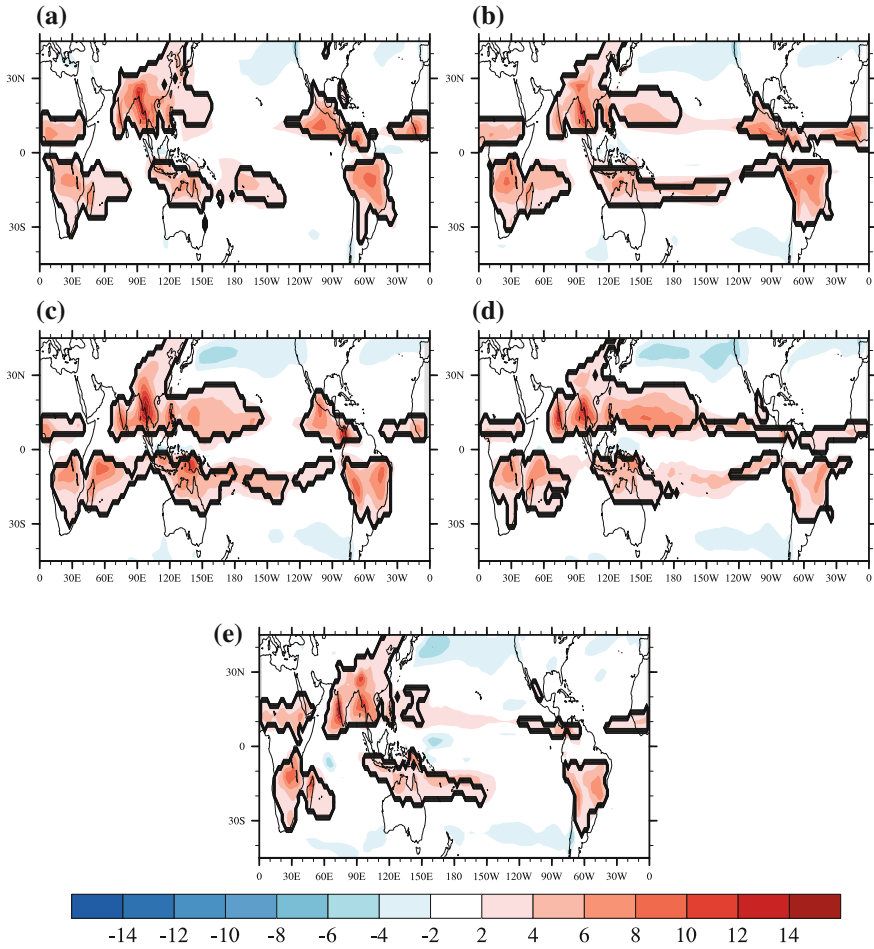


Fig. 1.5 Climatological annual range of precipitation (shaded; units: mm day^{-1}) and global monsoon domain (contours) derived from **a** GPCP, **b** MME of 21 climate models in CMIP5, **c** BCC_CSM T42, **d** BCC_CSM T106, and **e** BCC_CSM T266. The time periods are 1980–2007. The simulations are from the historical run of CMIP5 and BCC_CSM. The annual range is defined as the precipitation difference between local summer and winter, i.e., average precipitation from May to September (MJJAS) minus that from November to March (NDJFM) for the Northern Hemisphere, and average precipitation in NDJFM minus that in MJJAS for the Southern Hemisphere

monsoon region. However, the simulated NWP monsoon region and North American monsoon region in T266 are underestimated, suggesting that a tuning of the physical processes is needed when the model resolution is changed.

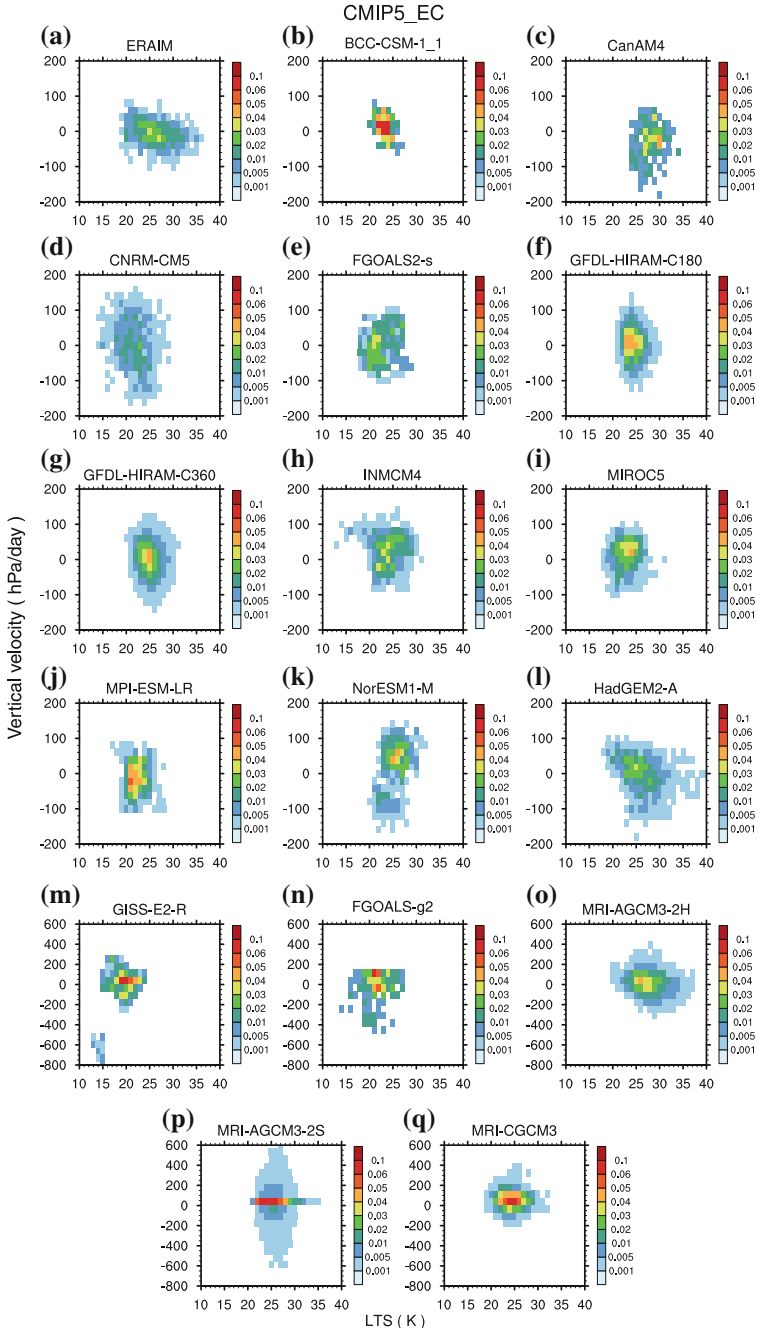
1.5.2.2 Metrics for Evaluating East Asian Cloud and Radiation

Differences in the climate sensitivity among models have long been attributed to the uncertainty in depicting the role of cloud (e.g., Cess et al. 1989; Senior and Mitchell 1993; Colman 2003). The Fourth Assessment Report (AR4) of the IPCC pointed out that there are large inter-model differences in cloud feedback (Randall et al. 2007), and that these differences are mostly attributable to the shortwave cloud feedback component. Stratus clouds play a dominant role in generating the shortwave cloud radiative forcing (SWCF; Zuidema and Hartmann 1995), and the associated errors should be quantified.

The East Asian continent is characterized by the most unique mid-topped stratus clouds during the boreal cold season (Yu et al. 2001, 2004), and is recognized—because of the inability to represent these clouds—as the region with one of the largest errors in the simulation of SWCF in CMIP3 and CMIP5 models (Zhang and Li 2013). These clouds are influenced by several large-scale controls (Zhang et al. 2013c), which are tightly correlated with the topographic effect downstream of the Tibetan Plateau.

Figure 1.6 shows the occurrence frequency of the environment fields sorted by low-troposphere stability (LTS; potential temperature difference between 500 and 850 hPa) and vertical speed at 700 hPa (ω_{700}) over East China derived from 16 CMIP5 models. Only samples in November–February are selected. The ranges of occurrence frequencies are widely different between models and the reanalysis. The vertical velocity in the reanalysis ranges within ± 100 hPa and the LTS ranges from 18 to 35 K. Most models have bins concentrated within small ranges of the LTS axis, which corresponds to the large differences in the LTS mean during the cold season (not shown). The ranges of ω_{700} also differ vastly among models. Five models' velocity axes are set from -800 to 600 hPa day^{-1} because of too much strong subsidence or ascending motion. The three MRI (the Meteorological Research Institute) models all have large ranges of vertical velocity. GISS_E2_R and FGOALS_g2 still show excessively strong rising motion (reaching -400 hPa day^{-1}). The above analysis indicates that the distribution of ambient field bins is vastly different among models. The distinction of East China lies in its geographic location, which is on the lee side of the Tibetan Plateau. The models exhibit quite different orographic effects, directly influencing the ambient fields.

SWCFs binned by two variables are described separately in Fig. 1.7. In the observation (Fig. 1.7a), intense SWCF mainly occurs in high stability (higher than 25 K) and ascending motion regimes, while low stability and subsiding regimes are associated with weak SWCF (the CERES data show this feature more clearly because of more samples). This is because low-level, large-scale lifting transports more moisture vertically and, along with the stable stratification, they jointly form a favorable environment for the maintenance of stratus. Therefore, the coexistence of high stability and low-level rising motion is important in forming strong SWCF. This response pattern helps us to examine whether models can simulate SWCF through a correct process.



◀ **Fig. 1.6** Occurrence frequency of low-troposphere stability (LTS; *horizontal axis*) and ω_{700} (*vertical axis*) bins over East China in CMIP5 models. Bin intervals are (a–l) 1 K for LTS and 20 hPa day⁻¹ for ω_{700} , (m–q) 1 K for LTS and 70 hPa day⁻¹ for ω_{700} . All ω_{700} axis ranges are from -200 to 200 hPa day⁻¹, except the last five models m–q whose ranges are from -800 to 600 hPa day⁻¹. All LTS axis ranges are from 10 to 40 K. All samples are November–February monthly means from 2001 to 2008. Reprinted from Zhang and Li (2013), with kind permission from Springer Science+Business Media

The contribution of rising motion to SWCF is evident. Intense SWCF in the model itself mainly occurs in the rising motion regime. However, the problems can be mainly attributed to three aspects. First, intense SWCF of the model itself occurs in relatively weaker LTS regimes, e.g., BCC_CSM_1.1, CanAM4, FGOALS_s2, GFDL_HIRAM_C180, HadGEM2_A, GISS_E2_R, and MRI_AGCM3_2h (s). For these models, the dependence of intense SWCF to strong LTS is not evident. Another problem is that intense SWCFs in some models (e.g., GISS_E2_R) are generated because of too much strong rising motion and can make the mean SWCF become closer to the observation, which, however, is not a correct process. Lastly, some models can simulate relatively similar response patterns, but the intense SWCF in the model itself is much lower than the observation (e.g., CNRM_CM5, MIROC5, MPI_ESM_LR, and MRI_CGCM3). Overall, there is no model that can reproduce an adequate response in terms of reflecting observational data.

Given the above biases associated with the stratus radiative effect in East China, to eliminate the biases associated with stratus simulations in this region, the topographic effect downstream of the Tibetan Plateau should be properly represented.

1.5.2.3 Metrics for Monsoon–ENSO Interaction

The interactions between El Niño and the East Asian–Western North Pacific (EA–WNP) monsoon include a series of complicated processes, in which Western North Pacific anticyclone (WNPAC) anomalies play a central role (Wu et al. 2009, 2010a; Wu and Zhou 2013, 2015). Therefore, the WNPAC during El Niño mature winter and decaying summer are taken as metrics to evaluate the three versions (T42, T106, and T266) of BCC_CSM in simulating the interactions between ENSO and EA–WNP monsoon.

To properly select simulated ENSO events, we apply EOF analysis to the monthly sea surface temperature anomaly (SSTA) in the tropical Pacific (20°N–20°S, 120°E–80°W) for all three versions of the model. Then, the December–February (DJF) mean of the obtained principal component (PC) time series is calculated. The years that the DJF-mean PCs are greater or less than 1 standard deviation are selected as strong El Niño or La Niña events, respectively. For the real world, we use five strong El Niño (1982, 1991, 1994, 1997, and 2002) and five La Niña events (1984, 1988, 1998, 1999, and 2007), with the DJF-mean Niño3.4 indices [area-averaged SSTA in (5°N–5°S, 170°–120°W)] greater or less than 1 standard deviation. For simplicity, we only analyze the composite results.

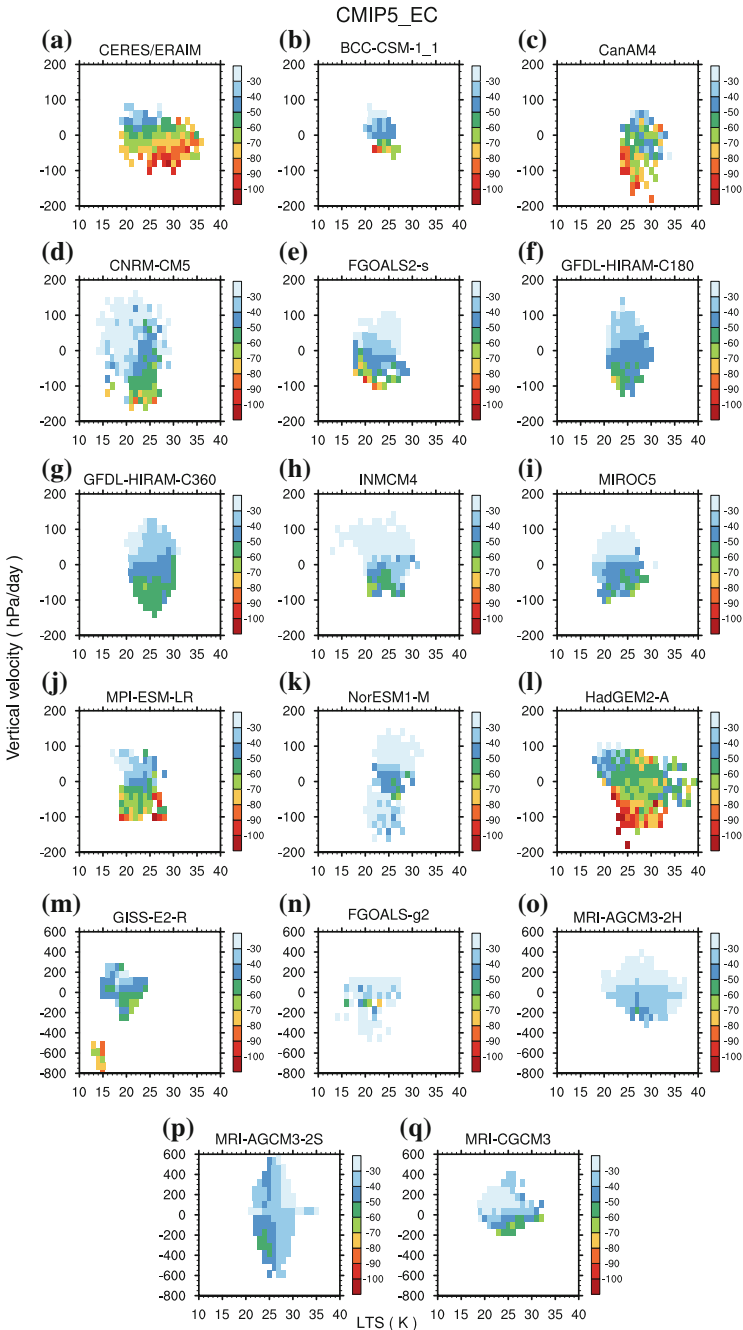


Fig. 1.7 Shortwave cloud radiative forcing binned by low-troposphere stability (*horizontal axis*) and ω_{700} (*vertical axis*) over East China in CMIP5 models. Bin intervals and axis ranges are all the same as in Fig. 1.6. All the samples are November–February monthly means from 2001 to 2008. Units: $W m^{-2}$. Reprinted from Zhang and Li (2013), with kind permission from Springer Science +Business Media

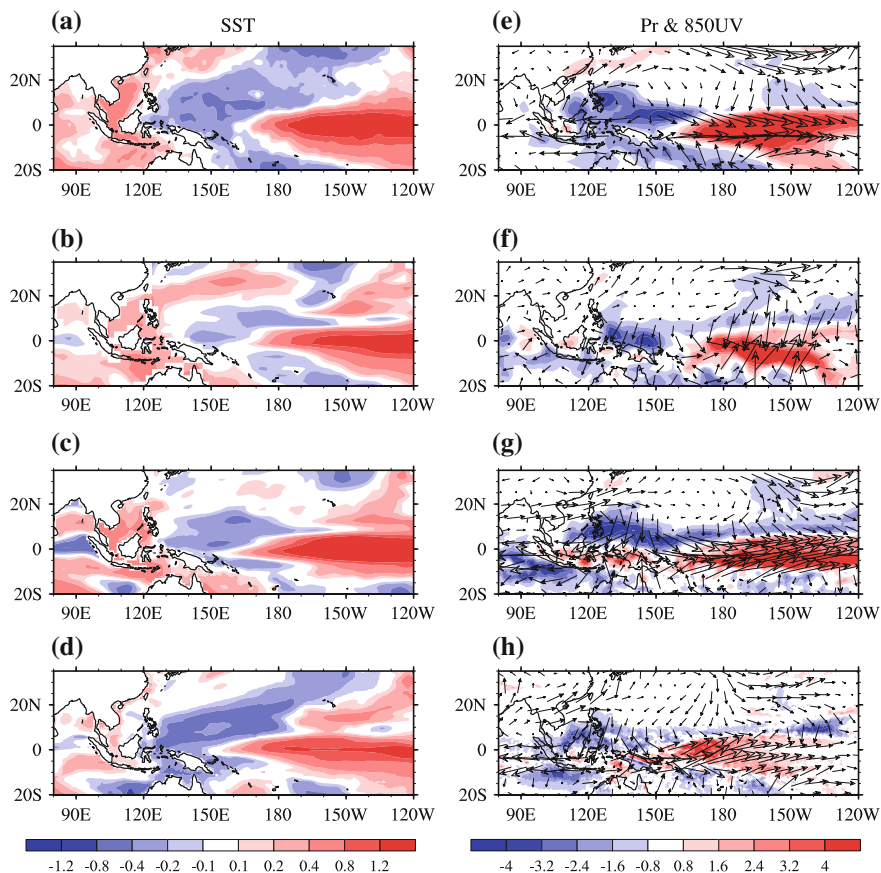


Fig. 1.8 SST anomalies during El Niño winter for the **a** observation, **b** T42, **c** T106, and **d** T266 versions of BCC_CSM. Panels **(e–h)** are the same as **(a–d)**, except for the precipitation and 850 hPa wind anomalies. For the observation, SST, precipitation, and circulation fields are derived from HadISST1.1, GPCP, and NCEP2 reanalysis, respectively

During El Niño mature winter, the WNPAC is coupled with underlying cold SST anomalies through a positive wind–evaporation–SST feedback (Fig. 1.8a, e; Wang et al. 2000). On the one hand, the cold SST anomalies suppress local convection, which further stimulates the Rossby-wave-like WNPAC to the west. On the other hand, the northeasterly anomalies to the southeastern flank of the WNPAC tend to enhance surface latent heat flux in situ and thus cool SST, because the WNP is dominated by the climatological trade wind. The WNPAC has large climate impacts. It tends to enhance precipitation over southeastern China and accelerate decay of El Niño (Wu et al. 2013).

The T42 and T106 versions of BCC_CSM simulate the WNPAC and associated negative precipitation and SST anomalies in situ, albeit the WNPAC is shifted

westward somewhat relative to the observation (Fig. 1.8b, c, f, g). The WNPAC in the T42 version is weaker than that in the observation, while that in the T106 version is stronger. Both the T42 and T106 versions do not simulate the anomalous precipitation belt extending from southeastern China to the south of Japan, and simulate only very weak precipitation anomalies to the northeast of Taiwan. For the T266 version, the anomalous anticyclone is completely shifted out of the WNP (Fig. 1.8h). Although the cold SST anomalies over the WNP are reproduced reasonably, the warm SST anomalies in the equatorial central-eastern Pacific and associated positive precipitation anomalies extend excessively westward. As a result, the cyclonic anomalies driven by the positive precipitation anomalies are shifted westward, which further push the WNPAC westward and out of the WNP.

During El Niño decaying summer, the WNPAC is maintained through the combined effects of local cold SSTAs and the remote forcing from the basinwide warming in the tropical Indian Ocean (IOBW; Fig. 1.9a, e; Wu et al. 2010a). The cold SST anomalies in the WNP remain from the preceding winter and spring, which tend to suppresses local convection and further excite the WNPAC to the

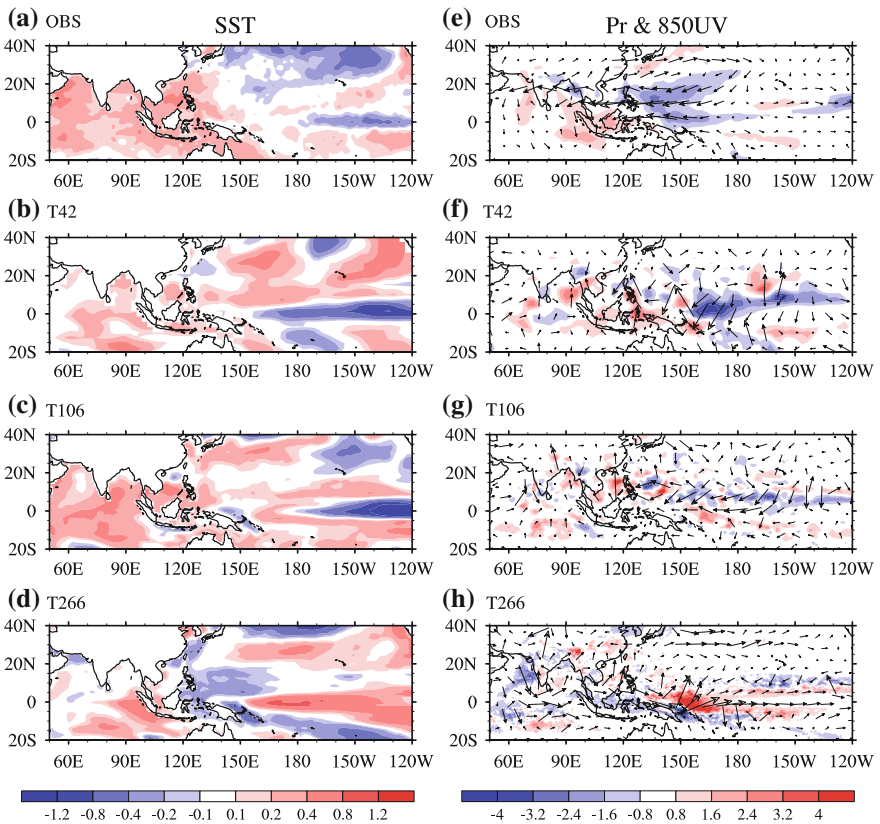


Fig. 1.9 As in Fig. 1.8, but for El Niño decaying summer

west. The IOBW tends to enhance local convection and further stimulate easterly Kelvin waves to the east. The off-equatorial anticyclonic vorticity anomalies associated with the Kelvin waves suppress local convection through causing boundary divergence. The suppressed convection stimulates Rossby-wave-like WNPAC to the west. The WNPAC corresponds to the westward extension of the Western Pacific subtropical high, and tends to intensify the Mei-yu precipitation during early summer (Fig. 1.9e).

For the T42 version, the anomalous anticyclone over the WNP is very weak (Fig. 1.9f). Correspondingly, highly sporadic in situ negative precipitation anomalies are not as well organized as those in the observation (Fig. 1.9b). The T42 model simulates the basinwide warming in the Indian Ocean, but fails to simulate the cold SSTAs in the WNP. Because of the weak anomalous anticyclone and weak Mei-yu precipitation in the climatology, this version of the model fails to simulate the positive precipitation anomalies extending from the middle and lower reaches of the Yangtze River to the south of Japan. The performances of the T106 version are similar to the T42 version (Fig. 1.9c, g).

The T266 version shows more severe simulation discrepancies. It fails to simulate the WNPAC (Fig. 1.9h). The WNP is covered by cyclone anomalies stimulated by the positive precipitation anomalies over the equatorial central Pacific. The discrepancy is caused by the false simulation of El Niño evolution. In the observation, El Niño tends to decay rapidly after the mature winter and evolve to a weaker La Niña during decaying summer. In contrast, the equatorial central-eastern Pacific is still dominated by the warm SSTAs during decaying summer in the T266 version (Fig. 1.9d). As a result, the T266 version fails to simulate the WNPAC and associated negative precipitation anomalies over the WNP, though it does simulate the cold SSTAs in the WNP and warm SSTAs in the tropical Indian Ocean.

In summary, having evaluated the relationships between ENSO and EA–WNP monsoon simulated by the three versions of BCC_CSM by taking the WNPAC as a metric based on its important roles in linking ENSO and monsoon, we can conclude that the T42 and T106 versions of the model reproduce the WNPAC in El Niño mature winter and decaying summer, albeit with several biases relative to the observation. However, the T266 (highest resolution) version fails to simulate the WNPAC in both seasons.

1.5.2.4 Metrics for Tropical Bias

Tropical biases are systematic errors in coupled GCMs found in multiple variables and at multiple timescales. In the present project, we focus on the most serious and long-lasting of these biases: the double Intertropical Convergence Zone (ITCZ) bias in the equatorial Pacific. Usually, the double ITCZ bias is represented by precipitation biases. A spurious rainfall belt can be found south of the equator in the models (e.g., Fig. 1.10b), where there is almost no rain (annual mean) east of 130° W in the observation (Fig. 1.10a). Because the SST is closely related to the

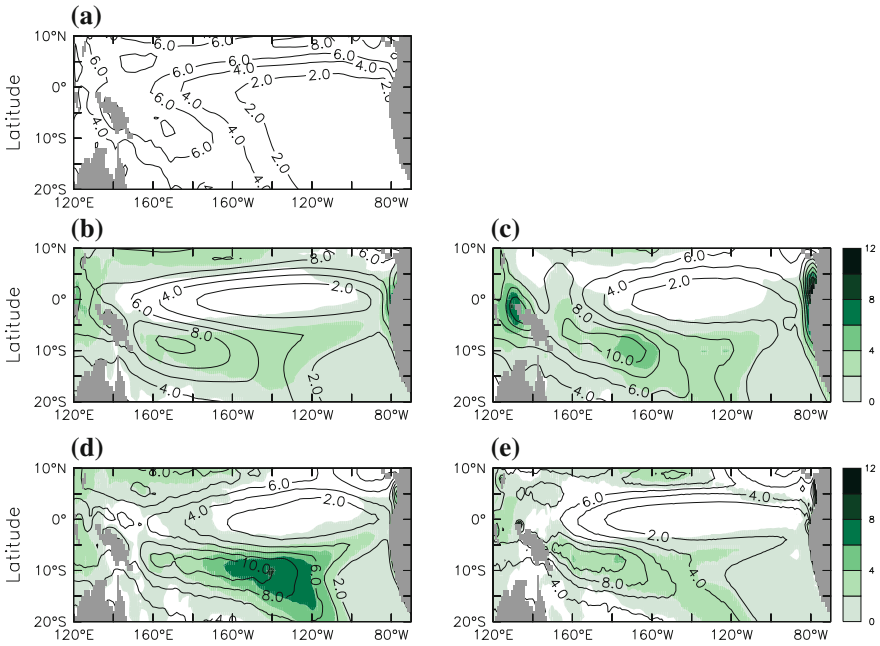


Fig. 1.10 Total precipitation in the equatorial Pacific for **a** GPCP, **b** CMIP5 multi-model ensemble, and three versions of the BCC_CSM: **c** T42; **d** T106; **e** T266 (contours). Shading in (**b**–**e**) indicates the biases of the models against GPCP. Units: mm day^{-1}

precipitation, and air–sea feedback plays an important role in the double ITCZ bias, we believe that the SST should also be evaluated along with the precipitation.

Figure 1.10 shows the precipitation in GPCP observations, the MME of 27 CMIP5 models, and the three versions of BCC_CSM (i.e., T42, T106, and T266). For the CMIP5 models, the biases are still there, but with slightly smaller magnitude compared to CMIP3 models (not shown). That is, there is no significant improvement between CMIP5 and CMIP3. The double ITCZ biases can also be found in all three BCC_CSM models, with magnitudes larger than the CMIP5 MME. Among the three versions, the high-resolution (T266) version is the best and the medium-resolution (T106) version is the worst. Therefore, there seems to be no significant relationship between the resolution and precipitation bias.

Figure 1.11 shows the SST in OISST observations, the CMIP5 MME, and the three BCC_CSM models. The T42 and T106 versions have warm SST biases in the eastern equatorial Pacific, while the T266 version has cold SST biases. This result also explains why the biases in the precipitation for the T266 version are the smallest. So, combining both the precipitation and SST results, we believe that the T42 version is still the best among the three models. This conclusion also suggests that the precipitation in T106 and the SST in T266 should be further tuned.

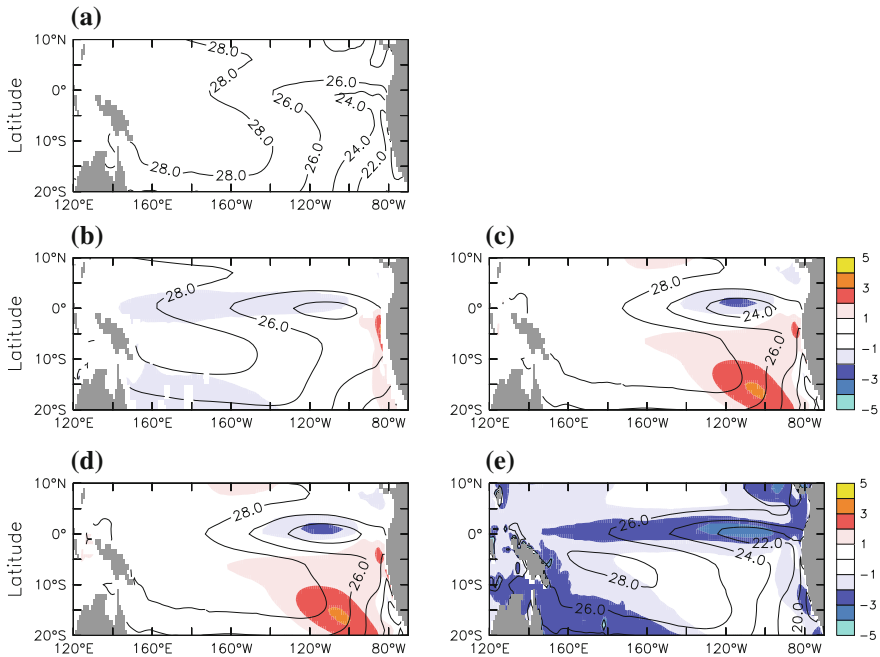


Fig. 1.11 As in Fig. 1.10, but for sea surface temperature. The observation is from OISST. Units: °C

1.5.2.5 Metrics for ENSO and the Aerosol Indirect Effect

ENSO is the dominant mode of interannual climate variability. It is characterized by an irregular period ranging between 2 and 7 years, an amplitude of sea surface temperature variation from 0.5 to 3 °C, a phase lock with a maximum in boreal winter, and a skewness toward El Niño. Although ENSO originates in the tropical Pacific, it affects the global climate and weather events such as drought/flooding and tropical storms.

For ENSO simulation, the CMIP5 MME shows some improvement compared to CMIP3, but there has been no major breakthrough and the multi-model improvement is mostly due to a reduced number of poor-performing models (Flato et al. 2013). For example, in CMIP3, the amplitude of ENSO ranged from less than half to more than double the observed amplitude (Guilyardi et al. 2009). By contrast, the CMIP5 models show less inter-model spread (Kim and Yu 2012), which is closely associated with more convergence in the strength of the seasonal cycle (Fig. 1.12), as the ENSO amplitude is an inverse function of the relative strength of the seasonal cycle. In two observational datasets, the percentage of total spectral energy due to the annual and semiannual cycles is 31 % for Hurrell et al. (2008), and 34 % for HadISST, leaving 69 and 66 % to the interannual signal, respectively. In CMIP3, this percentage, the relative strength of the seasonal cycle, varies from 0 %

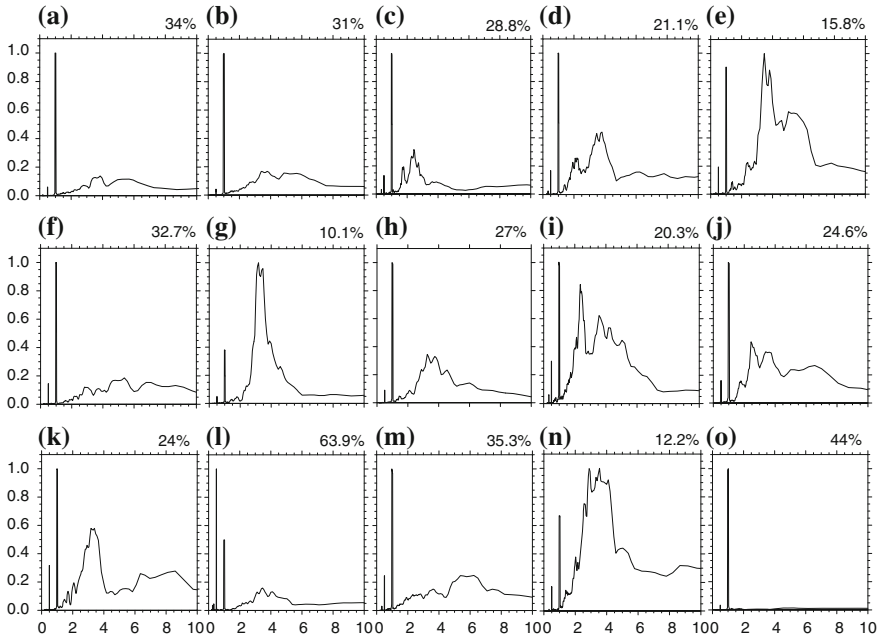


Fig. 1.12 Normalized power spectra of full monthly Niño3 sea surface temperature for observations [HadISST and Hurrell et al. (2008)] and 13 CMIP5 models' historical experiment runs. The value in the *top-left corner* of each *panel* is the percentage of total spectral energy in the annual and semiannual cycles

(FGOALS-g1) to 86 % (MIROC3.2-hires) (Guilyardi 2006), and most models underestimate the strength of the seasonal cycle, indicating that there are overestimations of the ENSO amplitude. In CMIP5, however, this amount ranges from 10 % (FIO-ESM) to 64 % (INMCM4), implying that there is more convergence in the seasonal cycle strength when compared to CMIP3. However, the convergence in CMIP5 ENSO amplitude is considered as error compensations because the wind–SST and shortwave–SST feedbacks are still poorly represented in CMIP5, as they were in CMIP3 (Bellenger et al. 2014).

On the other hand, there is large uncertainty in the representation of the aerosol indirect effect (AIE) in current climate models. For example, models have a tendency to overestimate the life cycle of sulfate aerosols in cloud, resulting in an overestimation of the direct and indirect effect of sulfate aerosols (Harris et al. 2013). Using a multiscale modeling framework model, Wang et al. (2011) found that conventional global climate models overestimate the AIE. Moreover, the uncertainty in the subgrid cloud parameterization can move into the scheme for aerosol–cloud interaction and affect the simulation of twentieth century warming (Golaz et al. 2011). Therefore, how to measure the strength of the AIE in CMIP5 models is an important but difficult topic.

Since the traditional approach to evaluating the strength of the AIE is not available to us due to the unavailability of direct variables and experiments in CMIP5 models, we need to define a metric to measure the strength of the AIE in the surface radiation budget. The word “indirect” in this sense means that the AIE perturbs surface radiation using cloud as the medium to take effect. Therefore, a variable reflecting the change in surface radiation in cloudy skies might be an ideal choice for our metric.

In the model, the surface downward shortwave radiation flux (FSDS) is the sum of the weighted mean of the clear-sky surface downwelling shortwave radiation flux (FSDSC) and the cloudy-sky surface downwelling shortwave flux (FSDSCL), with the weight being the cloud amount. In CMIP5 datasets, we can only obtain the total cloud amount (CLDTOT) rather than the cloud amount in every layer. So, as an approximation, we can deduce the FSDSCL by

$$\text{FSDSCL} = \frac{\text{FSDS} - \text{FSDSC} \times (1 - \text{CLDTOT})}{\text{CLDTOT}} \quad (1)$$

Although FSDSCL could also be influenced by the aerosol direct effect, our analysis shows that the trend of FSDSCL can still be used as a metric to measure the indirect effect, because the aerosol direct effect is not important in perturbing the northern Indian Ocean [NIO; (20°S–20°N, 50°–90°E)] surface radiation budget (Table 1.2; Hu et al. 2014).

From Table 1.2, although every model produces an SST increasing trend, the magnitude of the SST warming simulation is less than the observed [0.63 K (50 year)⁻¹]. We use 0.5 K (50 year)⁻¹ as the criterion to evaluate the ability of models in simulating the SST warming. Models that produce a greater than 0.5 K (50 year)⁻¹ SST increasing trend are classified as better models, and vice versa. Those models that simulate the SST increasing trend well (IPSL-CM5A-LR,

Table 1.2 Trends of annual mean clear-sky surface downwelling shortwave flux [FSDSC, W m⁻² (50 year)⁻¹], cloudy-sky downwelling shortwave radiation flux at the surface [FSDSCL, W m⁻² (50 year)⁻¹], surface downwelling shortwave flux [FSDS, W m⁻² (50 year)⁻¹], sum of net longwave flux, sensible and latent heat flux [ATM, W m⁻² (50 year)⁻¹], and SST (K) averaged over the northern Indian Ocean (20°S–20°N, 50°–90°E) during 1950–2000

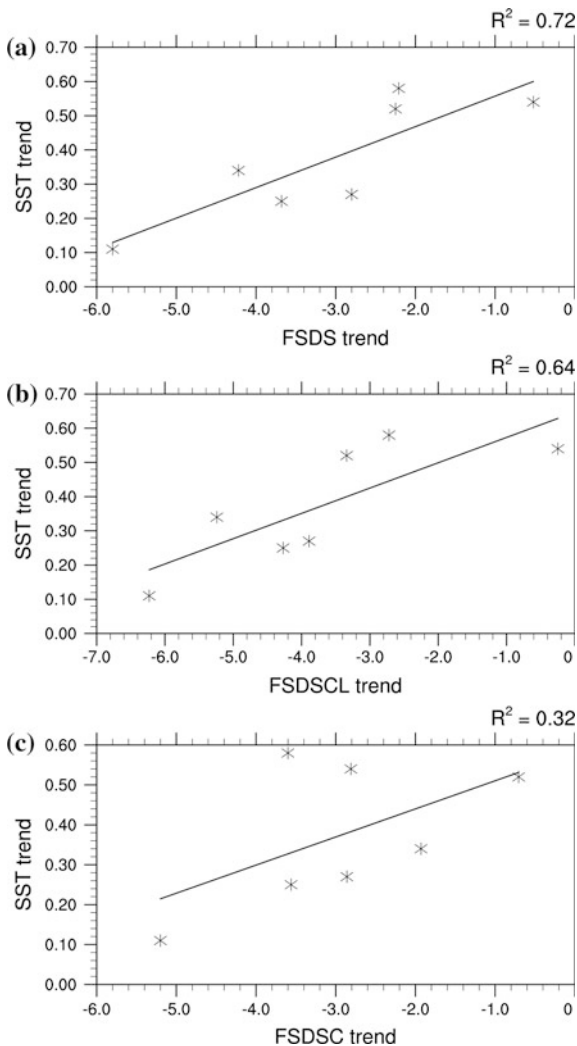
Model	ATM	FSDSC	FSDS	FSDSCL	FSDSCL (AA)	SST trend
GFDL-CM3	6.02	-5.20	-5.8	-6.23	-5.41	0.11
CSIRO-MK3-6-0	4.01	-3.56	-3.68	-4.27	-3.77	0.25
CESM-CAM5.1-FV2	2.81	-1.93	-4.22	-5.24	-3.41	0.34
NorESM1-M	3.31	-2.86	-2.8	-3.89	-4.99	0.27
IPSL-CM5A-LR	2.47	-3.60	-2.21	-2.72	-1.37	0.58
CanESM2	0.68	-2.81	-0.52	-0.25	-2.16	0.54
FGOALS-g2	2.74	-0.70	-2.25	-3.34	N/A	0.52
HadSST						0.63

FSDSCL (AA) is the trend for FSDSCL produced by anthropogenic-aerosol-only forcing simulations (Historical-AERO simulations). *Source* Hu et al. (2014)

CanESM2, and FGOALS-g2) produce a smaller FSDS decrease than those that do not. The sum of net longwave flux, sensible and latent heat flux (ATM in Table 1.2), which can be regarded as the heat flux to the ocean contributed by the atmosphere apart from solar radiation, contributes to the SST warming. However, the sum of these variables cannot explain well the differences in the SST trends among these models. Nevertheless, there is a good correlation between the trends of FSDSCL and SST in every CMIP5 model. That is, models that fail to simulate the SST increasing trend produce a significantly stronger FSDSCL decreasing trend than models that succeed. For example, in the standard historical simulation, the FSDSCL decreasing trend of GFDL-CM3 is the largest, reaching $-6.23 \text{ W m}^{-2} (50 \text{ year})^{-1}$, which contributes greatly to its FSDS decreasing trend of $-5.8 \text{ W m}^{-2} (50 \text{ year})^{-1}$. Thus, its corresponding SST increasing trend is only $0.11 \text{ K} (50 \text{ year})^{-1}$, which is the lowest value among the models. Models that fail to simulate the SST increasing trend also produce a larger magnitude of the FSDSCL decreasing trend in their corresponding Historical-AERO (only aerosol forcing) simulations, in agreement with the result from the standard historical simulation. These results indicate that the strength of the AIE plays an important role in a model's ability to simulate the NIO warming. Actually, although the FSDSC decrease in IPSL-CM5A-LR is the second largest among the models, due to its relatively weaker AIE characterized by its smaller FSDSCL decrease and much less total cloud amount, the model still produces the highest SST increase.

To further show the importance of the FSDSCL trend in driving the SST warming, we regress the SST increasing trend on the FSDS trend (Fig. 1.13a), FSDSCL trend (Fig. 1.13b), and FSDSC trend (Fig. 1.13c). The stronger the decreasing trend of FSDSCL is, the smaller the trend of SST increase. The regression coefficient passes the Student's *t*-test at the two-tailed 0.05 significance level, and the squares of correlation coefficient is as high as 0.64. These statistical results demonstrate that the trend of the FSDSCL, as a metric to measure the strength of the AIE, is an important contributing factor to the simulation of NIO warming. In contrast, if we regress the SST increasing trend to the FSDSC, the squares of correlation coefficient is only 0.32 and does not pass the statistical test. The regression of the SST trend on the FSDS is more deterministic, with the highest squares of correlation coefficient reaching 0.72. This is as expected, because the FSDS trend exerts a direct influence on the SST and is caused by both the aerosol direct and indirect effects. If we regress the FSDS trend on the FSDSC and FSDSCL trends separately, the FSDSCL trend can interpret 94 % of the FSDS trend, while the FSDSC trend interprets only 24 % of the FSDS trend (not shown). These results all indicate that the aerosol direct effect, by which FSDSC is mainly affected, is not important in affecting the FSDS and SST trends, whereas the AIE plays a more important role. This finding is consistent with the results of Dong and Zhou (2014). The aerosol's effect on the decadal phase change of the Pacific Decadal Oscillation (PDO) is further investigated by Dong et al. (2014). In addition, the effect of aerosol on long-term changes of East Asian summer monsoon is assessed by Song et al. (2014). Given the spread of climate models' response to

Fig. 1.13 Scatter plot of the trends of SST (y-axis) versus the trends of surface downward shortwave radiation flux (FSDS), cloudy-sky surface downwelling shortwave flux (FSDSCL), and clear-sky surface downwelling shortwave radiation flux (FSDSC) in seven CMIP5 models averaged over the northern Indian Ocean (20°S–20°N, 50°–90°E). *Source* Hu et al. (2014)



aerosol forcing, whether the aerosol’s effect on summer monsoon can serve as a metric for evaluating model performance deserves further study.

1.5.3 The MME Coupling Platform

1.5.3.1 Design and Implementation

Climate system models are a significant tool for forecasting and estimating future climate trends and abnormal events. Generally, such models couple together an

atmosphere, land surface, ocean, sea ice, and land-ice components. Classically, an intractable issue is the uncertainty caused by the errors intrinsic to each of these components. Furthermore, in certain highly coupled regions, these errors can be amplified and transmitted to other components, often augmented by increased iterations and the existence of feedback among the components. An interactive ensemble coupling model (IE model) is a useful method to reduce such stochastic perturbation. The IE strategy is different to the standard coupling (SC) strategy, which incorporates one member for each component linked by the coupler. The IE model involves adding multiple members of one component to the model, and the output fluxes of multiple members are averaged to be the mean values to force other components.

We have built an IE coupling platform based on NCAR CPL6 and CPL7, which are used widely in Standard Coupled (SC) climate models. To date, we have transported 15 interior components to the IE platform and designed a variety of experiments to test its validity. These experiments include simulations of the atmospheric components with multiple initial values, multiple physical processes, and multiple arguments based on the IE platform, simulations of multiple atmospheric members, and performance evaluations of multiple standalone coupling models on the same platform.

Our work on designing and developing the IE coupling platform includes the following main aspects.

With IE coupling platform, scientists can perform single experiment with multiple atmospheric models or multiple realizations of same atmospheric model. For other components in coupled simulation, we have designed two coupling schemes, which are the single and multiple land schemes. In the former, we average the fluxes from the atmospheric members and communicate them to the land, ocean, and sea ice components, while the latter has the same number of land instances as the atmospheric instances, in which each atmospheric instance is coupled with one realization of land surface component and the average fluxes from atmospheric and land instances will be delivered to the ocean and sea ice components.

To implement the IE coupling in traditional climate system model, we need to manage multiple atmospheric instances in one simulation first. The corresponding communication domain should be reallocated to support multiple atmospheric members. As the communication domain is represented by communicators, MPI communicators for each instance of atmospheric component have been generated and the correct communication relationship between each instance and the coupler has to be maintained carefully. Second, we have to keep copies of the communication identifier, grid dividing, and input arrays and output arrays for different atmospheric instance in coupler, so we can perform initialization, communication, run, and finalization of each atmospheric instance simultaneously during coupled simulation. To perform interaction between atmospheric instances and other single-instance components, the arithmetic mean values of the fluxes have been calculated before delivering them to different components. To keep better numerical accuracy, the averaging process involves dividing the result of each ensemble

component by the number of atmospheric instances, and then summing them up to produce the arithmetic mean.

By making use of the IE platform, we carried out a series of experiments to validate the implementation of IE platform, and to study the role of atmospheric noise and its climate effect. These experiments focused on numerical validation, evaluation, and comparison between the SC and IE models. With these experiments, we enable the quantitative study on the role of atmospheric noise and model uncertainty in coupled model. Multiple initial condition ensemble simulations show that stochastic noise generated by atmospheric dynamics is reduced and can be used to estimate the impact of atmospheric perturbations on the ocean and to identify the impact of atmospheric noise in complex sea–air coupling process; better reproduction of the relationship between ENSO and middle–high latitude SST in the North Pacific can be achieved compared to the original standard coupled model.

1.5.3.2 Portal

Besides designing and implementing the IE coupling platform, we have also developed a portal for the ensemble coupling platform, which is essentially a toolkit that can be used to optimize the performance of the IE model during runtime. The primary function of the portal is to provide a stable customized cluster environment. For supporting the ensemble coupling platform, the portal sets out to achieve two main goals: First, to provide an easy-use operation environment; second, to enhance the operability upon running the climate model. To maintain the reliability of the large-scale system at runtime, efforts have been made in two aspects. First, portal manages the hardware, software, and the application datasets in a unified way and keeps the information automatically synchronized throughout the whole system. Second, it incorporates a set of monitoring and diagnosis tools that can capture the events that occur during runtime. These events are divided into four categories, including the status of the hardware, the tasks and their status, the status of operating system, and the alarm messages from cluster environment. Regrouping their relationships and comparing them according to the time reference can help the manager and users identify the fault/problem since they are associated with related events.

Another important task of our portal is to implement the I/O optimization in order to relieve the I/O pressure on shared storage system. In traditional way, we run the application such as climate model on a shared storage. The shared storage resource might become a bottleneck of the system because of the pressure from serving large amount of concurrent I/Os and managing large number of files from quite a few users. To solve this issue, we have developed a storage tool which can mount/unmount different filesystems in real time and use different storage devices for read and write while keeping the unified logical filesystem view. This strategy can make best use of the bandwidth of parallel filesystems and also can protect the data of users from losing due to the instability of filesystem.

1.5.3.3 Performance Model and Process Layout Optimization for the Coupled Climate Model

In addition to the design and implementation of the ensemble coupling platform and its portal, a lightweight performance model is also necessary to help the user community improving the runtime performance. Climate simulations involve many complex physical processes interacting over a wide range of spatial and temporal scales, which leads to a significant increase in the demand for computing power (Gerber and Wasserman 2012). For example, the Community Earth System Model (CESM) accounts for nearly 50 % of the workload at the NCAR, and roughly \$250 000 will be saved by every 1 % improvement in computing performance, representing a significant return on investment (Srinath et al. 2014). This is the reason why performance tuning is needed to optimize the number of MPI processes for each component and the layout across these components in CESM.

A lightweight performance toolkit was proposed and implemented by extending four modules: Performance Model Builder, Layout Optimization, Layout Configuration, and Time Parser. The purpose of the toolkit is to identify the best process layout configuration for optimum performance improvement. The Performance Model Builder module and the Layout Optimization module are the core parts of the performance toolkit.

The Performance Model Builder module supports both online and offline services. It aims to determine the parameters of the performance model. The Layout Optimization module contains a load-balancing strategy to autotune CESM's layout. The strategy combines the deep first search (DFS) (Collin and Dolev 1994) and branch and bound ideology (Quesada and Grossmann 1992) to achieve maximum performance enhancement. Among the various elements that can impact the performance of the model, it is the process count, the number of coupled components, and the components' layout that are the three main factors of performance improvement, while the count of resources on a specific platform can also affect the performance characteristics of the model. An efficient and lightweight performance model helps guide the load-balancing decisions. We take the key factors of each component kernel into consideration and also involve the impact of the memory and communication bandwidth. This performance modeling approach can ensure the accuracy of the performance model as well as prevent the large overhead of fine-scale performance modeling.

Hence, we formulate the optimization problem as follows:

$$\min T_{\text{cesm}}(\text{components, layout, process_count})$$

The autotuning framework not only faces the challenge of the complexity of the coupled climate model itself, but also the complicated mixed integer nonlinear programming (MINLP) problem due to the various processor allocations with numerous layouts. Such a problem cannot feasibly be solved by a traditional optimization method with such huge solution space.

Table 1.3 shows the description of the performance model. From Fig. 1.14, the computation and communication performance of each component are the key factors in the performance model. As the resolution of the model increases, the computation power of each process first increases, and then becomes gentle as the cache miss rate rises and memory becomes the bottleneck.

The load-balancing strategy aims to autotune the CESM's layout optimization and identify the most feasible balancing scheme using branch and bound ideology and the DFS algorithm, thus efficiently reducing the memory and time cost. In order to reduce the communication overhead, we ensure that the unit of process allocated to each component is equal to the process number in each node. We regard the predicted time and the parallelism as the input and the component layout as the output. We select the control run experiment of the Fifth Assessment Report of the Intergovernmental Panel on Climate Change (IPCC AR5) experiments as our test case. Our tuning toolkit achieves a 58 % enhancement in performance on our two platforms, and the error is maintained at around 10 %.

1.5.3.4 Validation of the MME Coupling Platform

The CGCM model used is a variant of CCSM3.0, which has a different AGCM component. The AGCM model is version 2 of the Grid-point Atmospheric Model of LASG/IAP (GAMIL2.0) (Li et al. 2007, 2013). Other model components include CLM3.0 (Dickinson et al. 2006), version 1.4.3 of the Parallel Ocean Program (POP1.4.3), and version 5 of the Community Sea Ice Model (CSIM5). The model is hereafter referred to as the SC model (i.e., "standard coupling"). The IE model was constructed based on this SC model. Seven realizations of GAMIL2.0 with different initial conditions are coupled to a single realization of other model components in the IE system. The coupling between the multiple AGCMs and the other model components is accomplished by NCAR CPL6.

The SC model carried out an 850-year simulation with the external forcing fixed at preindustrial conditions. Over the last 450 years, the global-averaged SST was stable, with only a very small global-averaged trend (Zhang et al. 2014). The annual mean global-averaged sea ice extent showed a very small trend per century over the last 450 years. The SC model reached equilibration through this 850-year simulation. Therefore, the output of this preindustrial control run can be used to serve the initial conditions of the IE model in the interactive ensemble simulation.

In the IE model, there are seven AGCM realizations with different initial states, the ensemble mean of which is coupled with other model components. The IE platform is designed to reduce the atmospheric noise in the coupled climate system. Therefore, the IE model can be used to examine the variability with and without noise. Previous studies have used the IE strategy to investigate the SST variance in the North Pacific and North Atlantic, and found that the SST variance reduces in the IE model proportionally to the number of ensemble members of the atmospheric model (Yeh and Kirtman 2004; Wu et al. 2004). This indicates that most of the variability can be explained as the response to atmospheric stochastic forcing.

Table 1.3 Description of the performance model. Reprinted from Nan et al. (2014), with kind permission from IEEE

Component	Kernel	Computation characteristic	Communication characteristic	Performance model	
				Computation	Communication
POP	Baroclinic	Grid cells are the basic computing unit	Update halo	$T_{\text{comp}} = a * \text{block_size} + b$	$T_{\text{update_halo}} = (a * \text{Stotal} + b) / P$
	Barotropic		Global communication		
CAM	Dynamic		Update halo	$T_{\text{comp}} = (T_{12} * 12) / (P * (a * P + b))$	$T_{\text{update_halo}} = a * \text{Stotal} + b$
	Physics				
CICE	Dynamic		Update halo	$T_{\text{comp}} = (T_{12} * 12) / P$	$T_{\text{update_halo}} = a * P + b$
CLM			Global communication	$T_{\text{comp}} = (T_{12} * 12) / P$	$T_{\text{global}} = a * P + b$

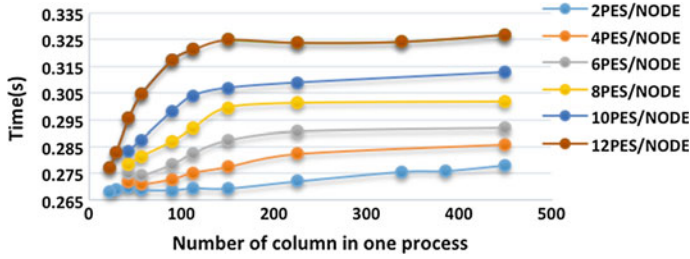


Fig. 1.14 Computational performance in CAM dynamics for 5 days running

Wu used a 100-year simulation of the IE model and SC model to verify the ratio of the SST variance between them (Xin et al. 2014a). The ratio of the SST variance between the IE and SC model showed that the IE model lowers the SST variance in most areas of the global ocean. The largest reduction of SST variance was in the North Pacific, North Atlantic, and southern tropical Pacific, where the value decreased by >90 %. Based on the previous study by Yeh and Kirtman (2004), over the region with values lower than 1/7 (0.14), the atmospheric noise plays a dominant role in SST variation. Therefore, our IE model also reflects the fact that the SST variability in the North Pacific and North Atlantic is determined by atmospheric noise. This indicates that the newly established IE platform is reasonably reliable.

The fluxes at the ocean–atmosphere interface are different between the IE and SC model. These fluxes include wind stress, heat fluxes (radiation heat flux and turbulent heat flux), and freshwater flux. Our result shows that the IE model decreases the variance of turbulent heat flux by >90 % northward of 40°N in the North Pacific, which is basically consistent with that of the SST. This indicates that the atmospheric noise forces the variation of SST through turbulent heat flux, and is in accordance with the conclusion of Zhang et al.(1998) and Li (2013) using a statistical method.

1.5.3.5 Application of the IE Model

The IE platform will couple multiple realizations of the AGCM to a single OGCM. The AGCM ensemble mean fluxes are used to drive the ocean model, while all atmospheric ensemble members experience the same ocean state produced by the OGCM. We validated that the IE model is useful in studying the role of atmospheric noise in SST variability. The IE procedure was designed to reduce or remove internal dynamic noise. Therefore, this IE model can be used for more studies on the influence of atmospheric noise and the interaction between the ocean and atmosphere. Below, we describe the results from some recent studies that have been carried out using the IE model.

Climate Impact of Atmospheric Noise

The climate impact of atmospheric noise is evident and the possible mechanism is discussed. When the IE model reaches a quasi-equilibrium state, surface temperature produced in the IE model is colder than that in the SC model. The cooling is moderate in the tropics and subtropics, but significant at the high latitudes in the Northern and Southern Hemispheres. The change is more pronounced at high latitudes because the atmosphere forces the ocean and the atmospheric perturbation is strong there. The significant differences between the IE platform and the SC model indicate that atmospheric turbulence at the air–sea interface can affect the coupled model’s performance in simulating surface temperature, especially at mid and high latitudes.

The dampened surface stress in the IE model suppresses oceanic mixing, which results in a thinner mixed layer. It is assumed that the deterministic part of the surface cooling is due to the reduced heat capacity of the mixed layer in high latitudes and the changed surface wind curl that causes upwelling/downwelling. The positive albedo feedback is responsible for the polar amplified changes. In order to adjust the surface energy budget, the ocean meridional overturning circulation is weakened, especially in the Atlantic, which further sustains the surface cooling. The model results suggest that the irregular ENSO cycle partly arises from the stochastic perturbation in the atmosphere. Comparison between the IE and the SC simulations also indicate the overestimated atmospheric perturbations in the SC model (Zhang et al. 2014).

Impacts of Atmospheric Noise on ENSO

The simulation of teleconnection between ENSO and global SST was compared between the SC and the IE model to investigate the impact of atmospheric noise on ENSO. The IE model highlights the out-of-phase relationship between ENSO and the SST in the mid and high latitudes of the North Pacific, while the SC model produces a positive correlation. This implies that the unreasonable simulation of atmospheric noise will influence the simulation of the variability of North Pacific SST by the SC model. The better simulation of ENSO and North Pacific mid–high latitudes SST by the IE model is consistent with that from the Ocean–Land–Atmosphere Studies (COLA) IE model (Kirtman and Shukla 2002). The COLA IE model also improves the simulation of the positive correlation in the tropical eastern Pacific, while it is not obvious in our IE model.

Further studies showed that the IE model better simulates the distribution of the Pacific–North American (PNA) teleconnection. The radiation and turbulent heat fluxes were also compared between the IE model and SC model. The results revealed that the correlation between radiation heat flux and Niño3.4 index in the IE model is negative in the midlatitudes of the North Pacific, which is consistent with the negative correlation between ENSO and SST. The better simulation of the PNA teleconnection was proposed to be the main reason for the good performance of the IE model in simulating the ENSO pattern.

The Role of Atmospheric Noise in NAO Variability

The IE model was studied in terms of the role of atmospheric noise in the NAO (Xin et al. 2014b). The NAO variance simulated by the SC model is weaker than in observations. The ensemble mean NAO variance of the IE model is much weaker than that simulated by the SC model. Since there are seven AGCM realizations in the IE model, there should be a 1/7th reduction in the NAO variance, when in fact it is about of 1/5. This indicates that ocean–atmosphere coupling and internal atmospheric noise work on the NAO together. The analysis of the variance showed that the contribution of external forcing from SST accounts for 7.7 % in the IE model.

The observed NAO shows a negative–positive–negative tripole pattern from the high latitudes to the subtropics over the North Atlantic Ocean. The ensemble (ENS) of the IE model shows weak correlation north of 40°N and statistically significant correlation south of 40°N. The correlation is positive from 25°N to 40°N and negative to the south of 25°N. This indicates a possible coupled variability between the NAO and SST in these regions.

In the Gulf Stream extension region, where the ocean dominates the SST variability, the cross-correlation between the NAO and SST in the IE model is much larger than in the SC model at lags from –1 to 5 months. The influence of the ocean on the NAO appearing in the Gulf Stream extension region is consistent with the result diagnosed from observational data using the Granger causality technique (Wang et al. 2004). In the IE model, when the atmospheric noise is reduced, the 1-month-lagged autocorrelation is 0.3, higher than in the SC model. The 2-month lagged autocorrelation is also significant at the 5 % level, while it is not significant in the SC model. This result is consistent with the longer memory of climate anomalies from the ocean–atmosphere coupling.

Currently, we are mainly analyzing the results of the experiment of multiple realizations of the same AGCM coupled with other model components. Actually, the IE platform has incorporated different AGCM models including the IAP AGCM model, the BCC AGCM model, and CAM5, as well as different OGCM models including the POP model, LICOM, and MOM. In the future, the IE model can serve a unified platform in comparisons between different climate models and different model components.

1.6 Concluding Remarks

This chapter provides an overview of the Chinese National Key Basic Research Project entitled “Development and Evaluation of High-Resolution Climate System Models” under grant no. 2010CB951900. After describing the background and objectives of the project, and introducing the organization of the four subprojects, the major achievements of the project after 5 years of research and development can be summarized as follows:

- (1) “One system” and “two platforms” have been developed. “One system” refers to the high-resolution modeling system, while “two platforms” refers to the multi-model ensemble coupling platform, and the model evaluation system.
- (2) The high-resolution modeling system includes the development of high-resolution component models and their corresponding coupled system. A fully coupled high-resolution climate system model (BCC_CSM2.0) has been established, with a horizontal resolution of T266 (approximately 45×45 km) for the AGCM and 30 km in the tropics for the OGCM. For multi-model ensemble purposes, the horizontal resolution of IAP AGCM has also been increased from $1.4^\circ \times 1.4^\circ$ to $0.5^\circ \times 0.5^\circ$. Along with the increases in model resolutions, both the dynamical core and physical processes of the component models have also been improved. A flexible leaping-point scheme, time-splitting methods, and two-dimensional parallel algorithm are employed in the dynamical core of the AGCM. The interactive CAR system has been fully evaluated and incorporated into the AGCM.
- (3) To facilitate interactive MME simulations and reduce model uncertainties, a flexible ensemble coupling platform has been studied and developed. The platform can perform the couple of the ensemble of multiple atmospheric models or multiple realizations of one atmospheric model with single ocean model in one experiment, which enables the quantification study on the role of atmospheric noise and model uncertainty in coupled model. Multiple initial condition ensemble simulations show that stochastic noise generated by atmospheric dynamics is reduced and can be used to estimate the impact of atmospheric perturbations on the ocean and to identify the impact of atmospheric noise in complex sea–air coupling process; better reproduction of the relationship between ENSO and middle–high latitude SST in the North Pacific can be achieved compared to the original standard coupled model.
- (4) Observational metrics for gauging model performance over the East Asian–Western Pacific domain have been developed. These metrics fall into four categories. The first is a set of metrics for the EASM, including its diurnal cycle, mean states, intraseasonal variation, interannual variability, interdecadal variability, and global monsoon context. The second is a set of metrics for East Asian cloud and radiation, including stratus cloud over East Asia, the divergence and stability of the atmosphere downstream of the Tibetan Plateau, and cloud radiation budgets. The third is a set of metrics for the tropical climate and tropical bias in coupled models, and the fourth is a metric for assessing the simulations of ENSO–monsoon interaction. In addition to these metrics having been used to gauge the performances of current state-of-the-art climate models, i.e., CMIP5 models, they have also been employed to assess the performance of the AGCM and corresponding coupled models developed in this project. Specifically, three versions of the AGCM in which the physical processes are identical but the resolution differs (i.e., T42, T106, and T266) have been examined and the added value of increased resolution identified. Weaknesses of the higher resolution models have also been discussed.

References

- Adler, R.F., et al.: The version-2 global precipitation climatology project 11 (GPCP) monthly precipitation analysis (1979–present). *J. Hydrometeorol.* **4**, 1147–1167 (2003)
- Barker, H. W., Pincus, R., Morcrette, J.J.: The Monte-Carlo independent column approximation: application within large-scale models. In: *Proceedings GCSS/ARM Workshop on the Representation of Cloud Systems in Large-Scale Models*, Kananaskis, Al, Canada, 10 pp (2002)
- Bellenger, H., Guilyardi, E., Leloup, J., Lengaigne, M., Vialard, J.: ENSO representation in climate models: from CMIP3 to CMIP5. *Climate Dyn.* **42**, 1999–2018 (2014). doi:[10.1007/s00382-013-1783-z](https://doi.org/10.1007/s00382-013-1783-z)
- Bleck, R.: An oceanic general circulation model framed in hybrid isopycnic–Cartesian coordinates. *Ocean Model.* **4**, 55–88 (2002)
- Cess, R.D., et al.: interpretation of cloud–climate feedback as produced by 14 atmospheric general circulation models. *Science* **245**, 513–516 (1989)
- Chen, H., Zhou, T., Neale, R., Wu, X., Zhang, G.: Performance of the New NCAR CAM3.5 in East Asian Summer Monsoon Simulations: Sensitivity to Modifications of the Convection Scheme. *J. Clim.* **23**, 3657–3675 (2010)
- Collin, Z., Dolev, S.: Self-stabilizing depth-first search. *Inf. Process. Lett.* **49**(6), 297–301 (1994)
- Colman, R.: A comparison of climate feedbacks in general circulation models. *Clim. Dyn.* **20**, 865–873 (2003)
- Dickinson, R.E., et al.: The Community Land Model and its climate statistics as a component of the Community Climate System Model. *J. Clim.* **19**, 2302–2324 (2006)
- Dong, L., Zhou, T.: The Indian ocean sea surface temperature warming simulated by CMIP5 models during the 20th century: competing forcing roles of GHGs and anthropogenic aerosols. *J. Clim.* **27**, 3348–3362 (2014)
- Flato, G., Marotzke, J., Abiodun, B., Braconnot, P., Chou, S.C., Collins, W., Cox, P., Driouech, F., Emori, S., Eyring, V., Forest, C., Gleckler, P., Guilyardi, E., Jakob, C., Kattsov, V., Reason, C., Rummukainen, M.: Evaluation of climate models. In: *Climate Change 2013: The Physical Science Basis. Contribution of Working Group I to the Fifth Assessment Report of the Intergovernmental Panel on Climate Change*. Cambridge University Press, Cambridge (2013)
- Gent, P.R., McWilliams, J.: Isopycnal mixing in ocean circulation models. *J. Phys. Oceanogr.* **20**, 150–155 (1990). doi:[10.1175/1520-0485\(1990\)020<0150:IMIOCM>2.0.CO;2](https://doi.org/10.1175/1520-0485(1990)020<0150:IMIOCM>2.0.CO;2)
- Gerber, R.A., Wasserman, H.J.: Large scale computing and storage requirements for biological and environmental science: Target 2017, DOE Office of Science, Office of Biological and Environmental Research, Office of Advanced Scientific Computing Research, and National Energy Research Scientific Computing Center. In: *Technical Report* (2012)
- Golaz, J.C., Salzmann, M., Donner, L.J., et al.: Sensitivity of the aerosol indirect effect to subgrid variability in the cloud parameterization of the GFDL atmosphere general circulation model AM3. *J. Clim.* **24**, 3145–3160 (2011)
- Griffies, S.M., et al.: Formulation of an ocean model for global climate simulations. *Ocean Sci.* **1**, 45–79 (2005)
- Guilyardi, E.: El Niño–mean state–seasonal cycle interactions in a multi-model ensemble. *Clim. Dyn.* **26**, 329–348 (2006)
- Guilyardi, E., Braconnot, P., Jin, F.F., Kim, S.T., Koliasinski, M., Li, T., Musat, I.: Atmosphere feedbacks during ENSO in a coupled GCM with a modified atmospheric convection scheme. *J. Clim.* **22**, 5698–5718 (2009)
- Harris, E., et al.: enhanced role of transition metal ion catalysis during in-cloud oxidation of SO₂. *Science* **340**, 727–730 (2013)
- He, C., Zhou, T.: The two interannual variability modes of the Western North Pacific Subtropical High simulated by 28 CMIP5-AMIP models. *Clim. Dyn.* (2014). doi:[10.1007/s00382-014-2068-x](https://doi.org/10.1007/s00382-014-2068-x)
- Hu, N., Li, L.J., Wang, B.: The role of aerosol indirect effect (AIE) in the northern Indian Ocean warming simulated by CMIP5 models. *Atoms. Ocean. Sci. Lett.* **7**, 411–416 (2014)

- Hurrell, J.W., Hack, J.J., Shea, D., Caron, J.M., Rosinski, J.: A new sea surface temperature and sea ice boundary dataset for the community atmosphere model. *J. Clim.* **21**, 5145–5153 (2008)
- IPCC: Climate Change 2013: The Physical Science Basis. Contribution of Working Group I to the Fifth Assessment Report of the Intergovernmental Panel on Climate Change. In: Stocker, T.F., Qin, D., Plattner, G.-K., Tignor, M., Allen, S.K., Boschung, J., Nauels, A., Xia, Y., Bex V., Midgley P.M. (eds.) Cambridge University Press, Cambridge, and New York, NY, 1535 pp (2013)
- Ji, J.: A climate-vegetation interaction model: Simulating physical and biological processes at the surface. *J. Biogeogr.* **22**, 2063–2069 (1995)
- Ji, J.J., Huang, M., Li, K.R.: Prediction of carbon exchange between China terrestrial ecosystem and atmosphere in 21st century. *Sci. China Ser. D: Earth Sci.* **51**(6), 885–898 (2008)
- Kanamitsu, M., Ebisuzaki, W., Woollen, J., Yang, S.-K., Hnilo, J.J., Fiorino, M., Potter, G.L.: NCEP-DOE AMIP-II reanalysis (R-2). *Bull. Amer. Meteor. Soc.* **83**, 1631–1643 (2002)
- Kim, S.T., Yu, J.Y.: The two types of ENSO in CMIP5 models. *Geophys. Res. Lett.* **39**, L11704 (2012). doi:[10.1029/2012GL052006](https://doi.org/10.1029/2012GL052006)
- Kirtman, B.P., Shukla, J.: Interactive coupled ensemble: a new coupling strategy for CGCMs. *Geophys. Res. Lett.* **29**(10), 5-1–5-4 (2002). doi:[10.1029/2002GL014834](https://doi.org/10.1029/2002GL014834)
- Large, W.G., McWilliams, J.C., Doney, S.C.: Oceanic vertical mixing: a review and a model with a nonlocal boundary layer parameterization. *Rev. Geophys.* **32**, 363–403 (1994)
- Li, Q., Sun, S.F.: Development and modification of a coupled soil-water-heat transfer common land model. *Sci. China Ser. D-Earth Sci.* **37**, 1522–1535 (2007). (in Chinese)
- Li, L.J., Wang, B., Wang, Y.Q., Wan, H.: Improvements in climate simulation with modifications to the Tiedtke convective parameterization in the grid-point atmospheric model of IAP LASG (GAMIL). *Adv. Atmos. Sci.* **24**, 323–335 (2007)
- Li, L.J., et al.: Evaluation of grid-point atmospheric model of IAP LASG, version 2.0 (GAMIL 2.0). *Adv. Atmos. Sci.* **30**, 855–867 (2013)
- Li, J., Yu, R., Yuan, W., Chen, H., Sun, W., Zhang, Y.: Precipitation over East Asia simulated by NCAR CAM5 at different horizontal resolutions. *J. Adv. Model. Earth Syst.* **7**(2), 774–790 (2015) doi:[10.1002/2014MS000414](https://doi.org/10.1002/2014MS000414)
- Liang, X.Z.: Description of a nine-level grid point atmospheric general circulation model. *Adv. Atmos. Sci.* **13**, 269–298 (1996)
- Liang, X.Z., Wang, W.C.: Cloud overlap effects on general circulation model climate simulations. *J. Geophys. Res.* **102**, 11 039–11 047 (1997)
- Liang, X.Z., Zhang, F.: Cloud-Aerosol-Radiation (CAR) ensemble modeling system. *Atmos. Chem. Phys.* **13**, 8335–8364 (2013)
- Lu, D., Zhou, T., Chen, X.: Changes of pacific decadal variability in the twentieth century driven by internal variability, greenhouse gases and aerosols. *Geophys. Res. Lett.* **41** (2014). doi:[10.1002/2014GL062269](https://doi.org/10.1002/2014GL062269)
- Ma, Q., Liu, X., Li, W.P., Ding, B.H.: Simulation of thermal and hydraulic properties affected by organic and gravel soil over the Tibetan Plateau during Summer. *Chin. J. Atmos. Sci.* **38**, 337–351 (2014). (in Chinese)
- Nan, D., Wei, X., Xu, J., et al.: CESMTuner: An auto-tuning framework for the community earth system model[C]. In: High Performance Computing and Communications, 2014 IEEE 6th Intl Symp on Cyberspace Safety and Security, 2014 IEEE 11th Intl Conf on Embedded Software and Syst (HPCC, CSS, ICESS), 2014 IEEE Intl Conf on. IEEE, pp. 282–289 (2014)
- Oleson, K.W., Dai, Y.J., Bonan, G., Bosilovich, M., Dirmeyer, P.: Technical description of the Community Land Model (CLM). NCAR Tech. Note TN-461 + STR, 174 pp (2004)
- Pincus, R., Barker, H.W., Morcrette, J.J.: A fast, flexible, approximate technique for computing radiative transfer in inhomogeneous clouds. *J. Geophys. Res.* **108D**, 4376 (2003). doi:[10.1029/2002JD003322](https://doi.org/10.1029/2002JD003322)
- Quesada, I., Grossmann, I.E.: An LP/NLP based branch and bound algorithm for convex MINLP optimization problems. *Comput. Chem. Eng.* **16**(10), 937–947 (1992)
- Räisänen, P., Barker, H.W., Khairoutdinov, M.F., Li, J., Randall, D.A.: Stochastic generation of subgrid-scale cloudy columns for large-scale models. *Q. J. Roy. Meteor. Soc.* **130**, 2047–2067 (2004)

- Randall, D.A., et al.: Climate Models and Their Evaluation. In: Solomon, S. et al. (eds.) *Climate Change 2007: The Physical Science Basis*. Contribution of Working Group I to the Fourth Assessment Report of the Intergovernmental Panel on Climate Change. Cambridge University Press, Cambridge (2007)
- Rayner, N.A., Parker, D.E., Horton, E.B., Folland, C.K., Alexander, L.V., Rowell, D.P., Kent, E.C., Kaplan, A.: Global analyses of sea surface temperature, sea ice, and night marine air temperature since the late nineteenth century. *J. Geophys. Res.* **108**, 4407 (2003). doi:[10.1029/2002JD002670](https://doi.org/10.1029/2002JD002670)
- Senior, C.A., Mitchell, J.F.B.: Carbon dioxide and climate. The impact of cloud parameterization. *J. Clim.* **6**, 393–418 (1993)
- Song, F.F., Zhou, T.J.: Interannual variability of East Asian Summer monsoon simulated by CMIP3 and CMIP5 AGCMs: skill dependence on Indian Ocean-Western Pacific Anticyclone Teleconnection. *J. Clim.* **27**, 1679–1697 (2014a)
- Song, F., Zhou, T.: The climatology and interannual variability of East Asian summer monsoon in CMIP5 coupled models: Does air-sea coupling improve the simulations? *J. Clim.* **27**, 8761–8777 (2014b)
- Song, F., Zhou, T., Qian, Y.: Responses of East Asian summer monsoon to natural and anthropogenic forcings in the 17 latest CMIP5 models. *Geophys. Res. Lett.* **41** (2014). doi:[10.1002/2013GL058705](https://doi.org/10.1002/2013GL058705)
- Srinath V., John, D., Youngsung, K.: Current efforts for performance analysis and enhancements of CESM, VESPAR, Oregon, USA, poster (2014)
- Sweby, P.K.: High-resolution schemes using flux limiters for hyperbolic conservation-laws. *SIAM J. Numer. Anal.* **21**, 995–1011 (1984)
- Sweeney, C., Gnanadesikan, A., Griffies, S.M., Harrison, M., Rosati, A., Samuels, B.: Impacts of shortwave penetration depth on large-scale ocean circulation and heat transport. *J. Phys. Oceanogr.* **35**, 1103–1119 (2005)
- Wang, B., Ding, Q.: The global monsoon: major modes of annual variation in Tropical precipitation and circulation. *Dyn. Atmos. Oceans* **44**, 165–183 (2008)
- Wang, B., Wu, R.G., Fu, X.H.: Pacific-East Asian teleconnection: How does ENSO affect East Asian climate? *J. Clim.* **13**, 1517–1536 (2000)
- Wang, W., Anderson, B.T., Kaufmann, R.K., Myeni, R.B.: The relation between the North Atlantic Oscillation and SSTs in the North Atlantic basin. *J. Clim.* **17**, 4752–4759 (2004)
- Wang, M., Ghan, S., Ovchinnikov, M., Liu, X., Easter, R., Kassianov, E., Qian, Y., Morrison, H.: Aerosol indirect effects in a multi-scale aerosol-climate model PNNL-MMF. *Atmos. Chem. Phys.* **11**, 5431–5455 (2011)
- Wu, T.W.: A mass-flux cumulus parameterization scheme for large-scale models: description and test with observations. *Clim. Dyn.* **38**, 725–744 (2012). doi:[10.1007/s00382-011-0995-3](https://doi.org/10.1007/s00382-011-0995-3)
- Wu, B., Zhou, T.J.: Relationships between East Asian-western North Pacific monsoon and ENSO simulated by FGOALS-s2. *Adv. Atmos. Sci.* **30**(3), 713–725 (2013)
- Wu, B., Zhou, T.: Relationships between ENSO and the East Asian-western North Pacific monsoon: observations versus 18 CMIP5 models. *Clim. Dyn.* (2015). doi:[10.1007/s00382-015-2609-y](https://doi.org/10.1007/s00382-015-2609-y)
- Wu, Z.H., Schneider, E.K., Kirtman, B.P.: Causes of low frequency North Atlantic SST variability in a coupled GCM. *Geophys. Res. Lett.* **31**, L09210 (2004). doi:[10.1029/2004GL019548](https://doi.org/10.1029/2004GL019548)
- Wu, T.W., Yu, R.C., Zhang, F.: A modified dynamic frame-work for the atmospheric spectral model and its application. *J. Atmos. Sci.* **65**, 2235–2253 (2008)
- Wu, B., Zhou, T., Li, T.: Seasonally evolving dominant interannual variability modes of East Asian climate. *J. Clim.* **22**, 2992–3005 (2009)
- Wu, B., Li, T., Zhou, T.: Relative contributions of the Indian Ocean and local SST anomalies to the maintenance of the western North Pacific anomalous anticyclone during El Nino decaying summer. *J. Clim.* **23**, 2974–2986 (2010a)
- Wu, T.W., Yu, R.C., Zhang, F., Wang, Z., Dong, M., Wang, L., Jin, X., Chen, D., Li, L.: The Beijing Climate Center atmospheric general circulation model: description and its performance for the present-day climate. *Clim. Dyn.* **34**, 123–147 (2010b). doi:[10.1007/s00382-008-0487-2](https://doi.org/10.1007/s00382-008-0487-2)
- Wu, T., et al.: Global carbon budgets simulated by the Beijing climate center climate system model for the last century. *J. Geophys. Res. Atmos.* **118**, 4326–4347 (2013). doi:[10.1002/jgrd.50320](https://doi.org/10.1002/jgrd.50320)
- Wu, T., et al.: An overview of BCC climate system model development and application for climate change studies. *J. Meteor. Res.* **28**(1), 34–56 (2014)

- Xin, X.G., Xue, W., Zhang, M.H., Li, H.M., Zhang, T., Zhang, J.: Simulation of SST variability in the North Pacific Ocean and ENSO by an interactive ensemble coupled model. *Chin. J. Geophys.* **57**(4), 1021–1031 (2014a). (in Chinese)
- Xin, X.G., Xue, W., Zhang, M.H., Li, H.M., Zhang, T., Zhang, J.: How much of the NAO monthly variability is from ocean–atmospheric coupling: results from an interactive ensemble climate model. *Clim. Dyn.* (2014b). doi:[10.1007/s00382-014-2246-x](https://doi.org/10.1007/s00382-014-2246-x)
- Yeh, S.-W., Kirtman, B.P.: The impact of internal atmospheric variability on the North Pacific SST variability. *Clim. Dyn.* **22**, 721–732 (2004)
- Yu, R.: A two-step shapepreserving advection scheme. *Adv. Atmos. Sci.* **11**(4), 479–490 (1994)
- Yu, R.C., Li, W., Zhang, X., Yu, Y., Liu, H., Zhou, T.: Climatic features related to eastern China summer rainfalls in the NCAR CCM3. *Adv. Atmos. Sci.* **17**: 503–518 (2000)
- Yu, R., Yu, Y., Zhang, M.: Comparing cloud radiative properties between the Eastern China and the Indian monsoon region. *Adv. Atmos. Sci.* **18**, 1090–1102 (2001)
- Yu, R.C., Li, J., Zhang, Y., Chen, H.M.: Improvement of rainfall simulation on the steep edge of the Tibetan Plateau by using a finite-difference transport scheme in CAM5. *Clim. Dyn.* (2015). doi:[10.1007/s00382-015-2515-3](https://doi.org/10.1007/s00382-015-2515-3)
- Yu, R., Wang, B., Zhou, T.: Climate effects of the deep continental stratus clouds generated by the Tibetan Plateau. *J. Clim.* **17**, 2702–2713 (2004)
- Zeng, Q., et al.: Documentation of IAP two-level atmospheric general circulation model. DOE/ER/60314-H1, TR044. 383 pp (1989)
- Zhang, H.: Development of IAP atmospheric general circulation model version 4.0 and its climate simulations. Ph.D. dissertation, Institute of Atmospheric Physics, Chinese Academy of Sciences, 194 pp (in Chinese) (2009)
- Zhang, Y., Li, J.: Shortwave cloud radiative forcing on major stratus cloud regions in AMIP-type simulations of CMIP3 and CMIP5 models. *Adv. Atmos. Sci.* **30**(3), 884–907 (2013)
- Zhang, X.H., Yu, Y.Q., Liu, H.: Wintertime North Pacific heat flux anomaly and air-sea interaction in a coupled ocean-atmosphere model. *Chin. J. Atmos. Sci.* **22**, 511–521 (1998). (in Chinese)
- Zhang, F., Liang, X.Z., Zeng, Q.C., Gu, Y., Su, S.J.: Cloud-Aerosol-Radiation (CAR) ensemble modeling system: overall accuracy and efficiency. *Adv. Atmos. Sci.* **30**, 955–973 (2013a)
- Zhang, F., Liang, X.Z., Li, J., Zeng, Q.C.: Dominant roles of subgrid-scale cloud structures in model diversity of cloud radiative effects. *J. Geophys. Res.* **118**, 7733–7749 (2013b)
- Zhang, H., Zhang, M., Zeng, Q.C.: Sensitivity of simulated climate to two atmospheric models: interpretation of differences between dry models and moist models. *Mon. Wea. Rev.* **141**, 1558–1576 (2013c)
- Zhang, Y., Yu, R., Li, J., Yuan, W., Zhang, M.: Dynamic and thermodynamic relations of distinctive stratus clouds on the lee side of the Tibetan Plateau in the cold season. *J. Clim.* **26**, 8378–8391 (2013d)
- Zhang, J., Xue, W., Zhang, M.H., Li, H.M., Zhang, T., Li, L.J., Xin, X.G.: Climate impacts of stochastic atmospheric perturbations at the ocean. *Int. J. Climatol.* (2014). doi:[10.1002/joc.3949](https://doi.org/10.1002/joc.3949)
- Zhou, T., Li, Z.: Simulation of the east Asian summer monsoon by using a variable resolution atmospheric GCM. *Clim. Dyn.* **19**:167–180 (2002)
- Zhou, T.J., Zhang, L.X., Li, H.M.: Changes in global land monsoon area and total rainfall accumulation over the last half century. *Geophys. Res. Lett.* (2008a). doi: [10.1029/2008GL034881](https://doi.org/10.1029/2008GL034881)
- Zhou, T.J., Yu, C.R., Li, H., Wang, B.: Ocean forcing to changes in global monsoon precipitation over the recent half-century. *J. Clim.* **21**(15), 3833–3852 (2008b)
- Zhou, T., Chen, X., Dong, L., Wu, B., Man, W., Zhang, L., Lin, R., Yao, J., Song, F., Zhao, C.: Chinese contribution to CMIP5: an overview of five Chinese Models' performances. *J. Meteorol. Res.* **28**(4), 481–509 (2014). doi:[10.1007/s13351-014-4001](https://doi.org/10.1007/s13351-014-4001)
- Zuidema, P., Hartmann, D.L.: Satellite determination of stratus cloud microphysical properties. *J. Clim.* **8**, 1638–1657 (1995)
- Zuo, R.T.: Development of new generation grid point atmospheric general circulation model with high resolution. Ph.D. dissertation, China People's Liberation Army University of Science and Technology, 328 pp (in Chinese) (2003)